Acta technologica agriculturae 2
Nitra, Slovaca Universitas Agriculturae Nitriae, 2012, p. 29–32

# FMECA METHOD ANALYSIS

# ANALÝZA METÓDOU FMECA

Marián BUJNA, Miroslav PRÍSTAVKA, Marek BURDA, Miroslav ŽITŇÁK

Slovak University of Agriculture in Nitra, Slovak Republic

Identifying risks and hazards in the production and non-production processes is a very important aspect not only from the moral but also financial point of view. It is now a priority in every organisation to identify potential imminent risk. Identifying risks and implementing corrective measures reduces costs and increases the quality of products and services offered by the company. One of the effective tools of risk analysis is the FMECA method. The method is based on determining the level of risk as a multiple of probability of failure origin, its importance and probability of failure detection. After identifying risks, corrective measures are proposed to reduce or completely eliminate any risk. Adding criticality evaluation of failures impact is the FMECA analysis method. This method is very effective. The objective of this paper is to apply the FMECA method to a selected part of the production process in OMS, spol. s r. o., a company which deals with manufacturing of lighting devices, as well as to identify major risks and propose corrective measures.

**Keywords:** risk, threat, FMECA method

Every organisation is faced with risks of different categories. Coordination of these risks is a decision-making process based on results of the risk evaluation process. Acceptance and implementation of the principle of risk assessment in the enterprise means a systematic solution of safety and health protection for its employees. For organisations this means optimizing the work process, reducing accidents and better quality of work.

People are facing various kinds of risks almost constantly throughout their lives. Nowadays, when the progress is always ahead, it is very important to identify risks in terms of quality offered.

FMECA is an analytical tool used to detect potential failures, their causes and effects. The task of this method is to determine the level of significance of different risks and measures for their elimination.

FMECA is a method that can be applied in various areas, mostly depending on the system being analysed and objectives. Firstly, it is used in the research of structural and procedural deficiencies of the analysed system. The method is applicable in all components of a safety management system: quality, the environment and safety.

In order to eliminate risks, the re-training of employees is conducted in the field of safety at work. In the stage of maintenance of equipment, FMEA can evaluate the biggest risk factors in ergonomy caused by poor working layout and elevated temperature in the workplace (Burda et al., 2011).

The purpose of this method is to highlight the importance of compliance with established rules and standards to enhance the needs of continuous improvement in environmental organisations, whatever their sphere of competence (Korenko et al., 2010).

The risk of individual operations is greatly reduced after applying corrective measures. Although the most risky operations will remain where they are, their risk level is reduced and it is the main objective of FMEA and FMECA (Paulíček et al., 2011).

FMEA can be a part of several methods. It is performed within a safety audit but also in case of the Poka Yoke method (Andrássyová et al., 2011; Kaplík et al., 2010).

The aim of this work is to identify and evaluate the risks and to suggest measures for reduction or a complete elimination of risks in the production process of OMS, spol. s r. o. which deals with manufacturing of lightning devices. A very important indicator is criticality. The manufacturing process is rather difficult because of a wide range of products the company offers. The FMECA method is very efficient for risk detection, which is also shown by results of practice, and it indicates a 70 % to 90 % success in detecting possible failures.

## Materials and methods

When resolving and formulating the risk analysis, it is important to distinguish between responsibility and competency. It is also necessary to obtain an overview about the organisational structure of the company.

Specification of potential failures and their causes, effects and criticality:

1. Responsibly of the FMEA team leader.
2. Responsibility matrix.
3. Commonly used words.
4. Succinct statement of the consequence of failures and signs.
5. Potential and typical failures.
6. Potential consequences of failures and their examples.
7. Potential causes of failures and their examples.
8. Classification of occurrence, significance and detectability of failures.
9. Priority number of risk – the product of occurrence, significance and detectability of failures.

Incidence – probability that a given specific cause/mechanism will occur. To estimate incidence we use a table according to STN IEC 60812.

Significance – a sign associated with the most critical consequences of a given failure type. It expresses a relative evaluation within FMEA. Significance is estimated according to IEC 60812.

Detection – a sign assigned to the best measures for detection. To determine its value, a table according to IEC 60812 is used.

The most important step before launching the FMECA method analysis is to choose the team leader who will be responsible for the entire process of analysis and the following tasks:

- to lead the team,
- to choose team members from various departments of the organisation,
- to secure required materials and statements,
- to follow the determined plan,
- to process forms accurately,
- to involve other specialists.

### Results processing

The results obtained will be processed in a form of FMECA analysis.

## Results and discussion

All computerised, manufacturing and measuring devices used in OMS ensure permanent quality of lighting fixtures that are distributed worldwide.

The options for transportation of materials on assembly lines without power drive are based on a hand-to-hand method.

Materials handling can be external or internal. While external handling is based on transmission from cell to cell, the internal one is based on transmission within the cell. In assembly operations, a layout system of LEAN cells is used. Their characteristic features are:

- small handling equipment,
- reduction of handling areas,
- tools and equipment are located as close as possible,

**Figure 1** Bend-cutting automatic line Salvagnini P4 S4
**Obrázok 1** Ohýbacio-vysekávacia automatická linka Salvagnini P4 S4

**Figure 2** Spraying line Ideal Line
**Obrázok 2** Striekacia linka Ideal Line

- no barriers along the way of an operator,
- flexibility, quick and easy reorganisation of the cell,
- semi-finished products and entering parts are stored close to the place of usage and achievable by the operator.

The FMECA team leader is responsible for:

- Security risks, consistent handling of the form and its delivery to the members concerned and cooperative sections.
- Team structure.
- Adherence to deadlines.

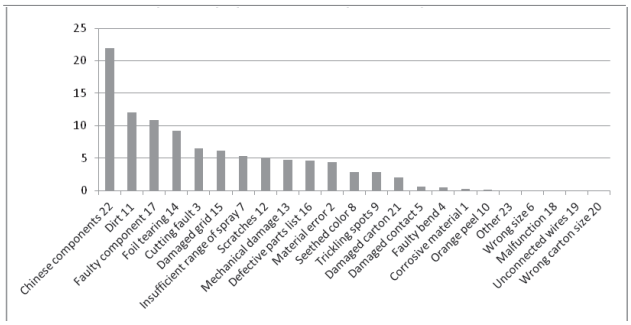


**Figure 3** Graphical display of failure in the production process in % 1
**Obrázok 3** Grafické zobrazenie chýb vo výrobnom procese v % 1
(1) korózia materiálu, (2) chyba materiálu, (3) chyba vysekávania, (4) chybný ohyb, (5) chybný spoj, (6) chybný rozmer, (7) nedostatok farby, (8) vyvretá farba, (9) stekance, (10) pomarančová kôra, (11) špina, (12) škrabance, (13) mechanické poškodenie, (14) zatrhávanie fólie, (15) poškodená mriežka, (16) chybný kusovník, (17) chybný komponent, (18) zlá funkcia, (19) nezapojené vodiče, (20) chybný rozmer krabice, (21) poškodená krabica, (22) čínske komponenty, (23) iné

**Table 1** Analysis of the production programme

| Level of selection (1) | Criteria for selection (2) | Characteristics of input selections (3) |
|---|---|---|
| Constructive | ⇨ form<br>⇨ dimensions<br>⇨ material<br>⇨ quality | ⇨ separation into the basic form and dimensional groups |
| Frequency | ⇨ series and repeatability<br>⇨ annual production capacity | ⇨ PQ diagrams, the relationship between assortment and capacity |
| Technological | ⇨ the sequence of production and cooperation<br>⇨ the amount and labour content of individual professions | ⇨ division into groups according to specifics<br>⇨ materials for production lines design |
| Capacitive | ⇨ total and partial capacity demands of individual technologies in the production system<br>⇨ limit values of external cooperation | ⇨ capacity demands of similar products<br>⇨ materials for the technology level analysis |

**Tabuľka 1** Analýza výrobného programu
(1) stupeň výberu, (2) kritéria pre výber, (3) charakteristika vstupných výberov

**Table 2** FMECA method analysis

| Potential consequences (1) | Importance (2) | Potential failure (3) | Potential failure causes (4) | Measures to reduce the occurrence (5) | Occurrence (6) | Control measures for detection (7) | Detection (8) | RPN (9) | Criticality (10) |
|---|---|---|---|---|---|---|---|---|---|
| Aesthetic defect with a significant impact on the function | 8 | ⇨ chinese component | ⇨ bad input material | ⇨ visual control | 8 | ⇨ multiple visual control | 7 | 448 | 6 |
| | | | | ⇨ proper handling of materials and compliance with established guidelines | 9 | ⇨ visual control at all levels of material handling | 4 | 288 | 7 |
| Aesthetic defect without affecting the function | 4 | ⇨ flowed colour | ⇨ application of thicker layer of paint | ⇨ output control in corpus packaging | 7 | ⇨ multiple visual control | 5 | 140 | 3 |
| | | | ⇨ too high temperature of calciner | ⇨ output control in packaging | 1 | ⇨ multiple visual control | 5 | 40 | 3 |
| Total failure of lamp functionality | 10 | ⇨ unconnected wires | ⇨ insufficient tightening of safety screw | ⇨ output control of insertion functionality | 2 | ⇨ introduction of continuous functionality control | 3 | 60 | 9 |
| | | | ⇨ poor removal of protective layer from a conductive part | ⇨ visual control at hourly intervals | 1 | ⇨ connections of electrical parts<br>⇨ inspection at more frequent intervals in comparison with a reference sample | 2 | 20 | 8 |

**Tabuľka 2** Analýza metódou FMECA
(1) možné dôsledky, (2) význam, (3) možná chyba, (4) možné príčiny chyby, (5) opatrenia k obmedzeniu výskytu, (6) výskyt, (7) kontrolné opatrenia k odhaleniu, (8) odhalenie, (9) rizikové číslo, (10) kritickosť

- Allocation of responsibilities of each task and informing decision-makers about the results obtained.

### Conclusion

As the OMS company does not use the FMECA method for risk assessment, this paper suggests a possible way of doing it. Each analysis requires teamwork when those involved try to detect and eliminate all deficiencies of the process researched in the earliest stages. Periodic reviewing and evaluating put the risks under control, and it is possible to monitor the rate of elimination or to eliminate the risks by means of corrective and preventive measures.

We had monitored the production of lightening fixtures in OMS, spol. s r. o. After performing the risks evaluation by the FMECA method, we found the Chinese component in optics to be the most common error in the manufacturing process. Less significant but rather frequent risks include failures caused by the finish. Negligible and rarely occurred risks when assembling the lighting fixtures include wrong wires connection or a faulty carton size. Each corrective measure contributes to the system security.

## Súhrn

Identifikácia rizika a ohrozenia vo výrobných ale i nevýrobných procesoch je veľmi dôležitý aspekt nielen z pohľadu morálneho, ale i finančného. V súčasnosti je takmer vo všetkých organizáciách prioritou odhaľovať potenciálne hroziace riziko. Odhaľovanie, identifikovanie rizika a zavádzanie nápravných opatrení znižuje náklady spoločnosti a zároveň zvyšuje kvalitu ponúkaných produktov a služieb. Jedným z účinných nástrojov na analyzovanie rizika je metóda FMECA. Metóda je založená na určení miery rizika ako súčinu pravdepodobnosti vzniku poruchy, významu poruchy a pravdepodobnosti jej odhalenia. Po identifikovaní rizika sa navrhnú nápravné opatrenia, ktorých úlohou je znížiť alebo úplne odstrániť riziko. Pridaním hodnotenia kritickosti dopadu chýb je hodnotenie metódou FMECA. Táto metóda je veľmi účinná. Cieľom práce je aplikovať metódu FMECA na vybranú časť výrobného procesu v spoločnosti OMS, ktorá sa zaoberá výrobou svietidiel, ako aj identifikovať najvýznamnejšie riziká a navrhnúť im nápravné opatrenia.

**Kľúčové slová**: riziko, ohrozenie, metóda FMECA

## References

ANDRÁSSYOVÁ, Z. – HRUBEC, J. – KOTUS, M. – DAŇKO, M. 2011. Application of method Poky Yoke in quality control. In Contemporary aspects of production engineering. Warszawa : Warsaw University of Life Sciences, 2011. p. 13 – 18. ISBN 978-83-928072-9-2.

BEDNÁROVÁ, P.2011. Dokumentácia rizík metódou posudzovania rizika FMECA vo vybranom podniku, 2011

BURDA, M. – ČIČO, P. – KOTUS, M. – DAŇKO, M. 2011. The risk assessment by FMEA at workplace. In Processes Improvement (Monography: Borkowski, S. – Stasiak-Betlejewska, R.). Trnava : Tripsoft, 2011. p. 116 – 125. ISBN 978-80-89291-40-3.

KAPLÍK, P. – BURDA, M. – KORENKO, M. 2010. Zlepšovanie kvality vo výrobnej organizácii prostredníctvom metódy Poka Yoke. In XII. medzinárodná vedecká konferencia mladých 2010 Nitra : SPU, 2010. p. 66 – 71. ISBN 978-80-552-0441-3.

KORENKO, M. – KAPLÍK, P. – BULGAKOV. 2010. Implementation of 5 S approach in the manufacturing organization V. In Naukovij visnik Nacionalnogo universitetu bioresursiv i prirodokoristuvanja Ukrajiny. – Kijiv : Nacionaľnyj Univesitet bioresurstv prirodokoritsuvanja Ukrajiny, 2010, 144, p. 59 – 64. častina 5.

PAULIČEK, T. – ČIČO, P. – ANDRÁSSYOVÁ, Z. – KOTUS, M. 2011. Analýza rizika procesu výroby. In Kvalita a spoľahlivosť technických systémov. Nitra : SPU, 2011. s. 52 – 56. ISBN 978-80-552-0595-3.

Contact address:
Ing. Marián Bujna, PhD., Department of Quality and Engineering Technologies, Faculty of Engineering, Slovak University of Agriculture, Tr. A. Hlinku 2, 949 76 Nitra, Slovak Republic, e-mail: marian.bujna@uniag.sk

Acta technologica agriculturae 2
Nitra, Slovaca Universitas Agriculturae Nitriae, 2012, p. 33–37

# DESIGN OF EQUIPMENT FOR DETERMINATION OF PERMEABILITY OF PACKAGE MATERIALS

# NÁVRH ZARIADENIA NA ZISŤOVANIE PRIEPUSTNOSTI OBALOVÝCH MATERIÁLOV

Stanislav ZEMAN, Ľubomír KUBÍK

Slovak University of Agriculture in Nitra, Slovak Republic

The paper deals with the design of equipment for the measurement of the gas permeability of packaging and mulching materials and the construction of the equipment. The design and construction of the equipment was performed according to the Standard EN STN 77 0333. The measurement of the permeability of oxygen through the polyethylene Bralen 2-63 with 9 % coloured concentrate Maxithen HP 533041 – violet foil was realized by means of a modified method. The measured permeability $P_x$ of oxygen through the foil of a thickness of 50 μm was 1 794.25 $cm^3.m^{-2}.d^{-1}.(0.1\ MPa)^{-1}$. The determined coefficient of permeability P was $4.2560.10^{-16}$ $mol.m^{-1}.s^{-1}.Pa^{-1}$, the coefficient of diffusion D was $4.3999.10^{-10}$ $m^2.s^{-1}$, and the solubility coefficient $S_p$ was $9.6735.10^{-7}$ $mol.m^{-3}.Pa^{-1}$.

**Keywords:** permeability, polyethylene foil, packaging, oxygen

Materials used at the packaging of foods are applied on the base of polymers in the present time. The protection of original quality of food against external undesirable effects is the function of packaging materials. The required protection of foods can be achieved with one layer of polymer, or in case of need, with a multilayer film, which includes different polymers, surface films and metallic foils. Barrier properties, i.e. protection of the package, are related mainly to the ability to transmit gases and vapours which damage the quality of the product. The dissipation of water may cause undesirable drying-out, which is manifested by the modification of the food structure. The moistening of food increases water activity and the state suitable for expansion of microorganisms is induced. Degradation processes of foods are dependent on time and temperature (Jasse et al., 1994; Ashley, 1985; Pye et al., 1976; Zeman a Kubík, 2007). We have to take into account all components of food during selection of package materials as well as the package material because they can react with one another under the impact of different storage conditions. Oxygen is harmful for foods of vegetal or animal origin. It causes the oxidation of higher fatty acids. The internal atmosphere of gases, such as $CO_2$ and $N_2$, is modified by preservation of the quality of foods (Jasse et al., 1994; Zeman a Kubík, 2007).

## Material and methods

### Fundamental principles of permeability

Sorption of gases and their transmission through the polymer depends on permeability and diffusion. The amount of gas $Q$ (mol), which is transferred through the membrane, is defined by the Equation (Jasse et al., 1994):

$$Q = \frac{D \cdot \sigma(p_1 - p_2) S \cdot t}{h} \quad (1)$$

where:

$D$ – coefficient of diffusion, $m^2.s^{-1}$
$p_1$ – external pressure, Pa
$p_2$ – internal pressure, Pa
$h$ – thickness of the membrane, m
$s$ – Henry's constant, $mol.m^{-3}.Pa$

On the assumption of thermodynamic equilibrium, the coefficient of permeability $P$ is given by the Equation:

$$P = D \cdot \sigma \quad (2)$$

We can also obtain the permeability of the membrane $P_x$ ($m^3.m^{-2}.s^{-1}.Pa^{-1}$) from the Equation:

$$P_x = P\frac{V}{Qh} \quad (3)$$

Fosse (2008) describes the characteristic of a lag time in the diffusion model. After using the separation of variables on the Fick's second law, imposing the initial conditions, and after calculating the limit for high times, we obtain:

$$\frac{c_h}{c_{h0}} = \frac{SD}{Vh}\left(t - \frac{h^2}{6D}\right) \quad (4)$$

where:

– $V$ is the ratio between the volume in the air chamber and the area of the fabric

This limiting equation revealed that there is the lag time for the system to reach the desired pseudo-steady state. The limiting equation also revealed that the permeability of the membrane can be found experimentally by calculating the best-fit slope of the equation. Similarly, the lag time $\Theta(s)$ can be found by experimentally calculating the x-intercept of the best-fit line of pseudo-steady state data points. The solubility coefficient $S_p$ ($mol.m^{-3}.Pa^{-1}$) can be calculated from the Equation (Brožová, 2008):

$$S_p = \frac{P}{D} \quad (5)$$

where:

$P$ – coefficient of permeability P, $mol.m^{-1}.s^{-1}.Pa^{-1}$
$D$ – diffusion coefficient, $m^2.s^{-1}$

The solubility coefficient Sp expresses the solubility of oxygen in the foil. Methods of determination of gas permeability

are described by Jasse et al. (1994); Pye et al. (1976); Koros et al. (1992); Sohail (1997) and Zeman a Kubík (2007). Polymeric materials present large-scale structures and properties which depend on their chemical structure, methods of preparation and conditions of processing. A significant participation of additives and application of polymer mixtures influence barrier properties of films through $CO_2$, $O_2$, $N_2$, or water vapours (Lee, 1980).

### Design of measurement equipment

Methods of detection and measurement for parameters of the permeability of packaging materials of gases are specified in the Standard EN STN 77 0333. The method was modified for conditions of our test. The permeability of gases is determined at barrier tests of materials as one of the specific parameter of the protective efficiency of the packaging. The design of the measurement equipment was projected. The design is considered universal for basic measurements. It represents sufficiently the principles of measurement and corresponds with the Standard EN STN 77 0333.

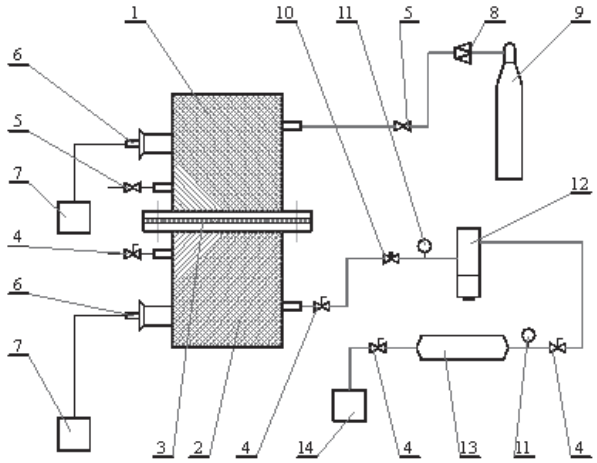


**Figure 1** Design of equipment for the measurement of gas permeability
1 – upper chamber, 2 – bottom chamber, 3 – membrane of the measured material, 4 – ball valve, 5 – needle valve, 6 – oxygen probe, 7 – digital oxygen meter, 8 – pressure control valve, 9 – pressure oxygen cylinder, 10 – one-way throttle valve, 11 – manometer, 12 – filter regulator, 13 – air tank, 14 – compressor

**Obrázok 1** Návrh zariadenia na meranie priepustnosti plynov
1 – horná komora, 2 – dolná komora, 3 – membrána meraného materiálu, 4 – guľový ventil, 5 – ihlový ventil, 6 – kyslíková sonda, 7 – digitálny oxygénmeter, 8 – redukčný ventil, 9 – tlaková kyslíková fľaša, 10 – jednosmerný škrtiaci ventil, 11 – manometer, 12 – regulátor s filtrom, 13 – vzdušník, 14 – kompresor

The diagram of design of the equipment for the measurement of gas permeability of packaging materials by means of an isobaric method is presented in Fig. 1, and the equipment is presented in Fig. 2. The bottom chamber (2) was firmly attached to the desk and the upper chamber (1) was attached above it by means of nuts. The tested material (3) was inserted between two chambers. A two-part test chamber was made of stainless steel and was resistant to corrosion and chemical effects. All parts of the chambers were equipped with the admission valve and the outlet valve (4, 5), as well as the outlet for insertion of the oxygen probe (6). The pressure oxygen cylinder (9) was used for the supply of pure oxygen (99.5 %). The amount of oxygen was adjusted by means of the pressure control valve in the upper chamber (1). The volume of each chamber was 1.128 $dm^3$. The diameter of the effective area between the chambers was 70 mm. The compressor (14) was used for the perfusion of the bottom chamber with the air. Adjusting of the air in this branch was integrated by means of the one-way throttle valve and the filter regulator (10, 12). The digital oxygen meters Mesura (7) were used for measuring the amount of diffused oxygen.

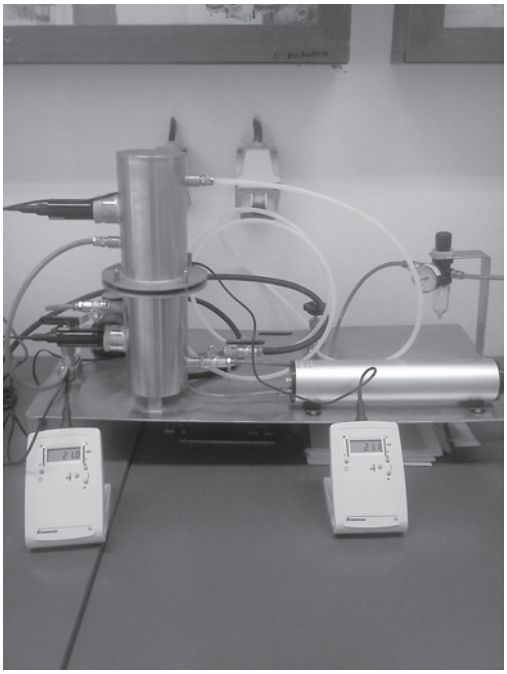

**Figure 2** Equipment for the measurement of gas permeability
**Obrázok 2** Zariadenie na meranie priepustnosti plynov

### Procedure of the test

The basis of the test with the isobaric method is to determine the concentration of the testing gas which diffused through the tested material from the chamber filled with a pure testing gas to the chamber with the air. Pressures of gases on both of them are equivalent. Samples have to be planar, pure and without mechanical damage. These samples are conditioned during 24 hours in laboratory conditions. Temperature and moisture are continually controlled. Dimensions of volumes $V_1$, $V_2$ and $S$ are determined before the test, where $V_1$ is the volume of the upper chamber of the testing vessel measured in $m^3$ with the precision of ± 5 %, $V_2$ is the volume of the bottom chamber of the testing vessel measured in $m^3$ with the precision of ± 5 %, and $S$ is the testing area of the sample measured in $m^2$.

Before the measurement, the upper chamber was perfused with the testing gas and the bottom chamber with the air as long as a homogenous environment was reached in each of both chambers. A suitable flow of both gases is about 600 $cm^3.min^{-1}$. The time of perfusion has to be at least 30 minutes and it is prolonged if the material is less permeable. The supply of the testing gas is stopped after perfusion, and all valves of both chambers are closed. The time of permeation of the testing gas through the sample is started in the moment. The diffusion of gas between both chambers is in progress for a period of 24 hours.

The coefficient of permeability $P$ was obtained from the increasing of the concentration $\Delta\rho_p$ ($m^3.kg^{-1}$) of the gas permeated through the foil into the calibrated volume $V$ in a time $\Delta t$ because the oxygen probes measured the relative

concentration of oxygen, and absolute values of concentration had to be calculated from tabulated values of the air and oxygen in real conditions. After applying the equation of state for ideal gas, the coefficient of permeability *P* can be obtained from the Equation:

$$P = \frac{\Delta\rho_p}{\Delta t}\frac{Vh}{S\rho_i}\frac{1}{RT} \quad (6)$$

where:

$\rho_i$ – density of gas in the initial volume V, kg.m$^{-3}$

$\Delta\rho_p$ – increasing of the density of gas transferred into the calibrated volume *V*, kg.m$^{-3}$

After applying Equation (3) and (6) and the equation of state for ideal gas $pV = nRT$, we can also obtain the permeability of the membrane $P_x$ (m$^3$.m$^{-2}$.s$^{-1}$.Pa$^{-1}$) from the Equation:

$$P_x = \frac{\Delta\rho_p VM}{\Delta t S\rho_i^2 RT} \quad (7)$$

where:

*M* – molecular mass, kg.mol$^{-1}$

## Results and discussion

The permeability of pure oxygen (99.5 %) through polyethylene foils of the thickness of 50 μm was measured. Samples of the foil contained 91 % of polyethylene Bralen RA 2-63 and 9 % coloured concentrate Maxithen HP 533041 – violet. Foils were made in the company Slovnaft, a.s., Bratislava, and the coloured concentrate was made in the company Gabriel-Chemie, Lázně Bohdaneč.

The conditions of measurement are described in Table 1. The measurement was performed at the temperature of 22 °C, 30 % of air moisture, and the barometric pressure of 102 600 Pa.

The measured quantities needed for calculating result quantities are presented in Table 2. Absolute values of densities were calculated from relative values measured by the oxygen probes. The oxygen probes were calibrated to the value of 20.9 % of oxygen in the air at the beginning of the test. The perfusion of the equipment by the air and oxygen during 30 minutes at the beginning of the test caused the increasing of initial values of the oxygen probes from 20.9 % to 23 % in the bottom chamber and to 98 % in the upper chamber. The value of 98 % of the amount of oxygen in the upper chamber is real, but the value of 23 % in the bottom chamber was occasioned by means of sensibility of the oxygen probe to the speed of the air flow.

The effect of time on the volume concentration of oxygen in the upper chamber during the test is presented in Figure 3. The effect of time on the volume concentration of oxygen in the bottom chamber during the test is presented in Figure 4. The coefficient of permeability P was calculated according to Equation (6). The permeability of the membrane Px was calculated from Equation (7).

**Table 1** Conditions of measurement

| Symbol (1) | Unit (2) | Quantity (3) | Description (4) |
|---|---|---|---|
| $V_1$ | m$^3$ | 0.0011283 | volume of upper chamber (5) |
| $V_2$ | m$^3$ | 0.0011283 | volume of bottom chamber (6) |
| $d_s$ | m | 0.07 | diameter of the foil sample (7) |
| *S* | m$^2$ | 0.0038465 | area of the foil sample (8) |
| *h* | μm | 50 | thickness of the foil (9) |
| *b* | Pa | 102 600 | barometric pressure of the air (10) |
| *T* | K | 295 | temperature of the air (11) |
| φ | % | 30 | relative moisture of the air (12) |
| M | kg.kmol$^{-1}$ | 32 | molar mass of $O_2$ (13) |
| R | J.kmol$^{-1}$.K$^{-1}$ | 8 314 | universal gas constant (14) |

**Tabuľka 1** Podmienky merania
(1) označenie, (2) jednotka, (3) veličina, (4) popis, (5) objem hornej komory, (6) objem dolnej komory, (7) priemer vzorky fólie, (8) plocha vzorky fólie, (9) hrúbka fólie, (10) barometrický tlak vzduchu, (11) teplota vzduchu, (12) relatívna vlhkosť vzduchu, (13) kilomólová hmotnosť $O_2$, (14) univerzálna plynová konštanta

**Table 2** Measured quantities

| Symbol (1) | Unit (2) | Quantity (3) | Description (4) |
|---|---|---|---|
| $\Delta_t$ | d | 1.0382 | time of the duration of permeation (5) |
| ρ | kg.m$^{-3}$ | 1.1965 | density of the air at the temperature of 295 K (6) |
| $\rho_{02}$ | kg.m$^{-3}$ | 1.3386 | density of $O_2$ at the temperature of 295 K (7) |
| $\phi_{102i}$ | % (vol.) | 98.0 | initial relative concentration of $O_2$ at the temperature of 295 K measured by the oxygen probe in the upper chamber (8) |
| $\rho_{102i}$ | kg.m$^{-3}$ | 1.3118 | initial density of $O_2$ at the temperature of 295 K measured by the oxygen probe in the upper chamber (9) |
| $\phi_{2021}$ | % (vol.) | 23.0 | initial relative concentration of $O_2$ at the temperature of 295 K measured by the oxygen probe in the bottom chamber (10) |
| $\rho_{2021}$ | kg.m$^{-3}$ | 0.2752 | initial density of $O_2$ at the temperature of 295 K measured by the oxygen probe in the bottom chamber (11) |
| $\phi_{2022}$ | % (vol.) | 23.7 | final relative concentration of $O_2$ at the temperature of 295 K measured by the oxygen probe in the bottom chamber (12) |
| $\rho_{2022}$ | kg.m$^{-3}$ | 0.2836 | final density of $O_2$ at the temperature of 295 K measured by the oxygen probe in the bottom chamber (13) |
| $\Delta\rho_{02p}$ | kg.m$^{-3}$ | 0.0084 | increasing of the density of $O_2$ at the temperature of 295 K in the bottom chamber (14) |

**Tabuľka 2** Merané veličiny
(1) označenie, (2) jednotka, (3) veličina, (4) popis, (5) doba trvania prestupu, (6) hustota vzduchu pri teplote 295 K, (7) hustota $O_2$ pri teplote 295 K, (8) počiatočná relatívna koncentrácia $O_2$ pri teplote 295 K meraná kyslíkovou sondou v hornej komore, (9) počiatočná hustota $O_2$ pri teplote 295 K meraná kyslíkovou sondou v hornej komore, (10) počiatočná relatívna koncentrácia $O_2$ pri teplote 295 K meraná kyslíkovou sondou v dolnej komore, (11) počiatočná hustota $O_2$ pri teplote 295 K meraná kyslíkovou sondou v dolnej komore, (12) konečná relatívna koncentrácia $O_2$ pri teplote 295 K meraná kyslíkovou sondou v dolnej komore, (13) konečná hustota $O_2$ pri teplote 295 K meraná kyslíkovou sondou v dolnej komore, (14) nárast hustoty $O_2$ pri teplote 295 K v dolnej komore

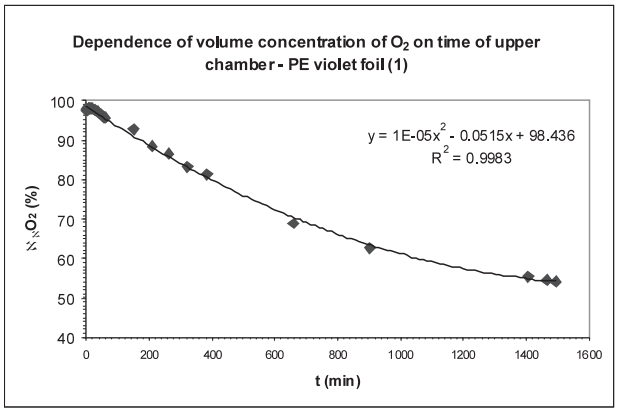


**Figure 3** Effect of time on the volume concentration of oxygen in the upper chamber during the test

**Obrázok 3** Závislosť objemovej koncentrácie kyslíka od času v hornej komore počas testu
(1) závislosť objemovej koncentrácie $O_2$ od času v hornej komore – PE fialová fólia

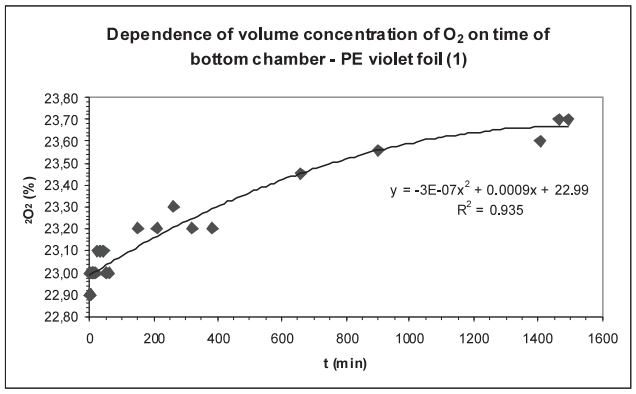


**Figure 4** Effect of time on the volume concentration of oxygen in the bottom chamber during the test

**Obrázok 4** Závislosť objemovej koncentrácie kyslíka od času v dolnej komore počas testu
(1) závislosť objemovej koncentrácie $O_2$ od času v dolnej komore – PE fialová fólia

The coefficient of diffusion $D$ of the membrane was determined from Equations (4) and (8). The solubility coefficient $S_p$ of the membrane was determined from Equation (5). The measured values from Table 1 and Table 2 were used for calculation. The time lag Θ was calculated by performing the linear regression analysis only with data points that contribute to the pseudo-steady state. The model implied the regression

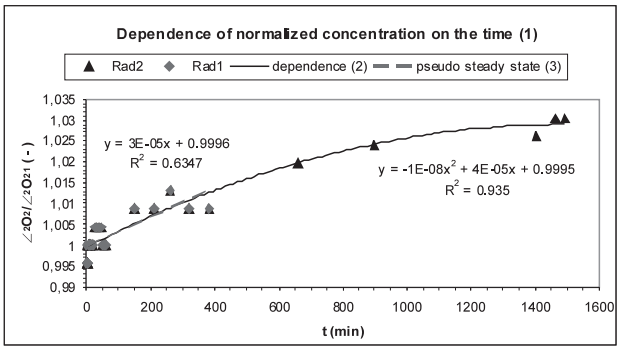


**Figure 5** Effect of time on the normalised concentration

**Obrázok 5** Závislosť normalizovanej koncentrácie od času
(1) závislosť normalizovanej koncentrácie od času, (2) závislosť, (3) pseudo-rovnovážny stav

should be linear and the general form was $y = b + ax$, where a and b were estimated on the base of Equations (4), as it is presented in Figure 5. The tangent in Figure 5 represents the pseudo-steady state and its slope represents the slope of Equation (4). Then, the diffusion coefficient $D$ is determined:

$$D = \frac{Vha}{S} \tag{8}$$

where:
$a$ – slope

Results of transport coefficients of oxygen through the PE foil are presented in Table 3. Transport properties are also related to the thickness of the foil. The polyethylene Bralen 2-63 with 9 % coloured concentrate Maxithen HP 533041 – violet foil shows high values of coefficients. The foil is highly permeable for oxygen. Bhadha (1999) presents values of the coefficient of permeability P (mol.m.m$^{-1}$.s$^{-1}$.Pa$^{-1}$) in the range from 0.4120 to 0.0375. The foil is not very suitable for food packaging but it is suitable for the mulching of plants.

## Conclusion

The design of the equipment for measuring the gas permeability of the packaging material was realized and the equipment was constructed. The design and construction of the equipment was performed according to the Standard EN STN 77 0333. The measurement of the permeability of oxygen through the polyethylene Bralen 2-63 with 9 % coloured concentrate Maxithen HP 533041 – violet foil was realized. Measurements and calculations of permeability were modified

**Table 3** Transport properties of the polyethylene Bralen 2-63 with 9 % coloured concentrate Maxithen HP 533041 – violet foil for oxygen permeability, thickness of the foil 50 μm

| Transport properties (1) | Experimental values (6) | Experimental values related to the foil thickness (7) | |
|---|---|---|---|
| Coefficient of permeability $P$ (2) in mol.m$^{-1}$.s$^{-1}$.Pa$^{-1}$ | 4.2560. 10$^{-16}$ | coefficient of permeability P (2) in mol.m.m$^{-1}$.s$^{-1}$.Pa$^{-1}$ | 1.8387.10$^{-15}$ |
| Permeability $P_x$ (3) in cm$^3$.m$^{-2}$.d$^{-1}$.(0.1MPa)$^{-1}$ | 1794.2500 | permeability $P_x$ in cm$^3$.m.m$^{-2}$.s$^{-1}$.Pa$^{-1}$ | 0.1038 |
| Coefficient of diffusion (4) in m$^2$.s$^{-1}$ | 4.3999.10$^{-10}$ | coefficient of diffusion (4) in m$^3$.s$^{-1}$ | 2.2000.10$^{-14}$ |
| Solubility coefficient Sp (5) in mol.m$^{-3}$.Pa$^{-1}$ | 9.6735.10$^{-7}$ | solubility coefficient $S_p$ (5) in mol.m.m$^{-3}$.Pa$^{-1}$ | 4.8368.10$^{-11}$ |

**Tabuľka 3** Transportné vlastnosti polyetylénovej fólie Bralen 2-63 s 9 % farebným koncentrátom Maxithen HP 533041 – fialový, pre priepustnosť kyslíka, hrúbka fólie 50 μm
(1) transportné vlastnosti, (2) koeficient priepustnosti, (3) priepustnosť, (4) koeficient difúzie, (5) koeficient rozpustnosti, (6) experimentálne hodnoty, (7) experimentálne hodnoty vztiahnuté k hrúbke fólie

and a personal approach was applied. The modified measurement enabled to obtain experimental values comparable with other authors. Measurements confirmed that the designed equipment is suitable for measuring the permeability of oxygen, but the improvement of the measurement of gas concentration will be needed for measuring the absolute concentration of gases.

## Súhrn

Práca sa zaoberá návrhom zariadenia na meranie priepustnosti plynov cez obalové a mulčovacie materiály a konštrukciou zariadenia. Návrh a konštrukcia zariadenia boli realizované na základe aplikovania normy EN STN 77 0333. Boli realizované merania priepustnosti pre kyslík cez polyetylénovú fóliu Bralen 2-63 s 9 % farebným koncentrátom Maxithen HP 533041 – fialová fólia, pomocou modifikovanej metódy. Bola stanovená priepustnosť $P_x$, 1794,25 $cm^3.m^{-2}.d^{-1}.(0,1\ MPa)^{-1}$ pre kyslík cez fóliu hrúbky 50 μm. Bol tiež stanovený koeficient permeability P, $4,2560.10^{-16}$ $mol.m^{-1}.s^{-1}.Pa^{-1}$, koeficient difúzie D, $4,3999.10^{-10}$ $m^2.s^{-1}$ a koeficient rozpustnosti kyslíka vo fólii Sp, $9,6735.10^{-7}$ $mol.m^{-3}.Pa^{-1}$.

**Kľúčové slová:** priepustnosť, polyetylénová fólia, balenie, kyslík

## References

ASHLEY, R. J. 1985. Permeability and plastics packaging. In J. Comyn (ed), Polymer Permeability. London : Elsevier Applied, p. 269 – 308.

BHADHA, M. P. 1999. How weld hose materials affect shielding gas quality. In Welding Journal, 1999, no. 2, p. 35 – 40.

BROŽOVÁ, L. 2008. Měření permeability kyslíku u fólií pro uchování a ochranu archiválií. Ústav makromolekulární chemie, AV ČR, [online] Publikované: 11. 4. 2011. [citované 26.3.2012]. Dostupné z http://www.nkp.cz/restauratori/2008/Vavrova_Ohlidalova_2008.pdf, s. 7 – 14.

JASSE, B. – SEUVRE, A. M. – MATHLOUTHI, M. 1994. Food Packaging and Preservation. Blakie Academic and Professional an imprint of Champan & Hall, Glasgov, London, 1994, 275 p. ISBN 07514 01182 X.

FOSSE, E. 2008. Estimating Lag Time and Permeability in Membranes. [online] Publikované: 30.5.2008. [citované 26.3.2012]. Dostupné z http://www.math.hmc.edu/~levy/181_web/Fosse_ web. .pdf, s. 1 – 14.

KOROS, W. J. – COLEMAN, M. R. – WALKER, D. R. B. 1992. Controlled permeability polymer membranes. In Annu. Rev. Mater. Sci., 1992, no. 22, p. 47.

LEE, W. M. 1980. Selection of Barrier Materials from Molecular Structure. In Poly. Eng. Sci., 1980, no. 20, p. 65 – 69.

PAUL, D. R. – KEMP, D. R. 1973. The diffusion time lag in polymer membranes containing adsorptive fillers. In Journal Polymer, Sci., 1973, no. 41, p. 79 – 93.

PYE, D. G. – HOEN, H. H. – PANAR, M. 1976. Measurement of gas permeability of polymers. In Journal Appl. Polym. Sci., 1976, no. 20, p. 287 – 301.

SOHAIL, H. – JACK, Y. 1997. ATR-FTIR spectroscopic studies of the structure and permeability of sulfonated poly (ether sulfone) membranes. In Journal Chem. Soc., Faraday Trans., 1997, no. 93. p. 1613 – 1620.

EN STN 77 0333: 1987, Determination of gas permeability of packaging materials.

ZEMAN, S. – KUBÍK, Ľ. 2007. Investigation Methods of Polymeric Packaging Materials Permeability. In Acta technologica agriculturae, vol. 10, 2007, no. 3 – 4, p. 93 – 97. ISSN 1335-2555

Contact address:
doc. Ing. Stanislav Zeman, PhD., Department of Production Engineering, Faculty of Engineering, Slovak University of Agriculture in Nitra, Tr. A. Hlinku 2, 949 76 Nitra, Slovak Republic, tel.: +421 37 6414 300, fax: +421 37 7417 003, e-mail: Stanislav.Zeman@uniag.sk
RNDr. Ľubomír Kubík, PhD., Department of Physics, Faculty of Engineering, Slovak University of Agriculture in Nitra, Tr. A. Hlinku 2, 949 76 Nitra, Slovak Republic, tel.: +421 37 6414 879, fax: +421 37 7417 003, e-mail: Lubomir.Kubik@uniag.sk

Acta technologica agriculturae 1
Nitra, Slovaca Universitas Agriculturae Nitriae, 2012, p. 38–40

# THREE-YEAR STUDY ON SOIL ROUGHNESS UNDER THE CONTROLLED TRAFFIC SYSTEM

# SLEDOVANIE VYROVNANOSTI POVRCHU PÔDY V RÁMCI SYSTÉMU CTF V TROJROČNOM EXPERIMENTE

Jana GALAMBOŠOVÁ, Vladimír RATAJ, Lukáš VELČICKÝ

Slovak University of Agriculture in Nitra, Slovak Republic

Controlled traffic farming is a technology which minimises the compacted area of a field by establishing permanent tramlines. Up to date, applications are combined with the no-till technology mainly. There is no evidence about effects of CTF on soil roughness. A three-year study was conducted to assess the effect of the implemented CTF system on the soil surface roughness at a 16 ha field. A CTF field and a control field were compared each season. Based on results, it can be concluded that CTF did not cause any problems in terms of the quality of the soil surface. The roughness of the CTF and control field was not statistically different, except of one year with the difference of 0.018 m, which is from practical point of view negligible. The coefficient of variation was acceptable and ranged from 2.18 to 6.37 % for the CTF field and from 2.25 to 4.69 % for the control field.

**Keywords:** controlled traffic farming, tillage, soil roughness

Soil compaction is one of the most important problems of current land management due to the size of machinery and uncontrolled traffic at fields. In traditional farming, there is more than 80 % of the field trafficked (Kroulik, 2009). Controlled traffic farming (CTF) is the technology which minimises the compacted area of the field. All operations over years are conducted in one direction using permanent tramlines. Up to date, applications are combined with the no-till technology mainly (Chamen, 2006). There is no evidence about effects of CTF in combination with conventional or minimum tillage.

Despite of many advantages (Yule, 2006 and others), CTF has still not been widely used in Europe. There are still barriers of CTF implementation in Eastern Europe. These can be summarised as follows:

- high precision of satellite guidance (RTK) is required, used with integrated autopilots, there is not many of them in usage yet,
- in order to avoid high soil roughness, there is a very strictly used practice to conduct some field operations angle-wise to the previous one (especially stubble tillage after harvest),
- a lot of farmers still use traditional tillage with a plough (Galambošová a Rataj, 2010).

Because of the absence of knowledge on soil roughness under the CTF system, the three-year study was conducted at Kolíňany University Farm.

Soil roughness can be characterised as the difference of the soil surface from an ideal straight line parallel to the surface. There are different methods used to assess soil roughness, e.g.:

- non-contact lased prophilograph (Mayer et al., 2010),
- geodetic total station (Anken et al., 2007),
- mechanical prophilograph (Garcia Moreno et al., 2008).

The value of soil roughness can be then expressed as the coefficient of variance or standard deviation.

## References

The controlled traffic system was implemented at a 16 ha field "Pri Jeleneckej ceste" in spring 2009. Details of the system are

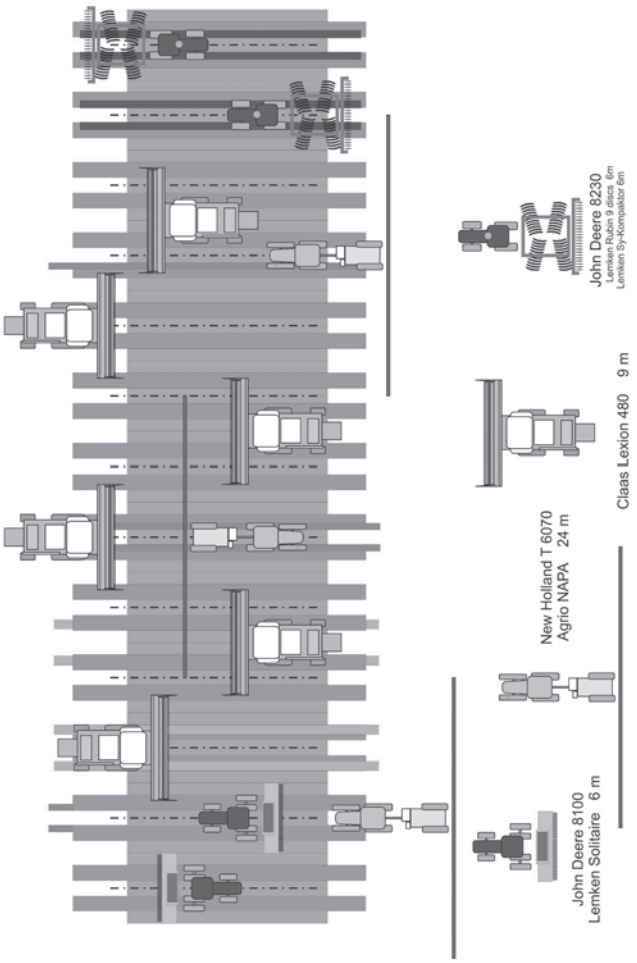


**Figure 1** Layout of the machinery movement during the long-term experiment
**Obrázok 1** Schéma pohybu strojov v rámci experimentu

**Table 1** Machinery used within the CTF system

| No (1) | Machinery (2) | Operation (3) | Implement width (4) |
|---|---|---|---|
| 1 | John Deere 8230 + Lemken Sy-Kompaktor + Lemken Rubin | seedbed preparation(5) stubble tillage (6) | 6 m |
| 2 | New Holland T 6070 with RTK satellite guidance (7) + Lemken Solitaire 9 | drilling (8) | 6 m |
| 3 | New Holland T 6070 + Agrio NAPA | spraying (9) | 24 m |
| 4 | Claas Lexion 480 | harvesting (10) | 9 m |

**Tabuľka 1** Technika využívaná v rámci systému CTF
(1) číslo, (2) strojová súprava, (3) operácia, (4) šírka záberu, (5) predsejbová príprava, (6) podmietka, (7) s RTK presnosťou, (8) sejba, (9) postrekovanie, (10) zber

described in Galambošová and Rataj (2010). Machinery used for field operations are given in Table 1 and the design of the system is given in Figure 1.

In order to assess the effect of CTF on soil roughness, measurements were taken during three seasons after stubble tillage as follows:

A. In 2009 measurements were after stubble tillage after spring barley harvest. The Lemken Rubin disc harrows were used for the tillage operation, conducted in the same direction as the crop was drilled at the controlled traffic field and angle-wise at the control field. Measurements were carried out at 31 monitoring points of the CTF field and 20 monitoring points of the control field. The distance from a horizontal level panel to the soil surface was measured 57 times at each monitoring point.
B. Oil seed rape was grown at the CTF field in 2010. Again, stubble tillage was conducted with Lemken Rubin. There were 19 monitoring points used at the CTF field and 20 monitoring points at the control field for measurements. The laser device BOSCH DLE 150 mounted on a portable tripod (Figure 2) was used for measurements. At each point, 42 measurements were taken.
C. In 2011 winter wheat was grown under the CTF system. Stubble tillage was conducted in the same pattern as in the last two years. Soil roughness was measured based on the methodology described for year 2010 (Figure 2).

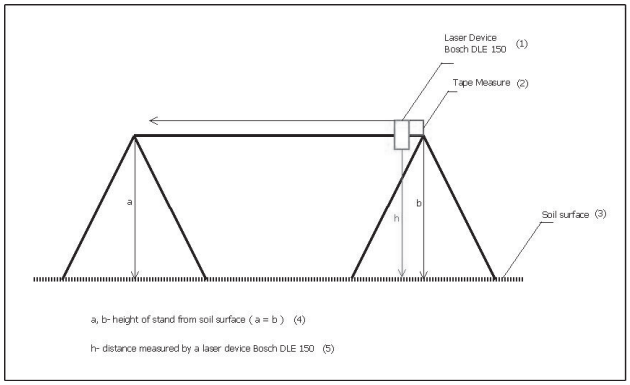


**Figure 2** Scheme of the device used for soil roughness measurements
**Obrázok 2** Schéma zariadenia využívaného na meranie vyrovnanosti povrchu pôdy
(1) laserový diaľkomer Bosch DLE 150, (2) meter, (3) povrch pôdy, (4) chýba, (5) meraná vzdialenosť

### Evaluation of the data

All data obtained at a monitoring point were averaged and then statistically analysed. Data sets were tested for equality of variances with the F-test. If variances are assumed to NOT be equal, the t-test that assumes non-equal variances will be used, and vice versa.

As an indicator of soil roughness, the coefficient of variation was calculated and compared as well.

## Results and discussion

Based on the methodology, data were measured each year after the stubble tillage operation. For each monitoring point data were averaged and these were used for statistical analyses. Basic statistics of measurements are given in Table 2, 3 and 4 for years 2009, 2010 and 2011, respectively. The measured parameter "*h*" stands for the distance from the horizontal level ("zero" level) to the soil surface (Figure 2).

**Table 2** Basic statistic of the values of "*h*" in 2009

| Parameter *h* (1) | CTF field (2) | Control field (3) |
|---|---|---|
| Mean in cm (4) | 8.43 | 8.25 |
| Standard deviation in cm (5) | 0.54 | 0.39 |
| Minimum in cm (6) | 7.39 | 7.48 |
| Maximum in cm (7) | 9.68 | 8.78 |
| Count (8) | 31 | 20 |

**Tabuľka 2** Popisná štatistika parametra "*h*" pre rok 2009
(1) parameter, (2) CTF parcela, (3) kontrolná parcela, (4) priemer, (5) smerodajná odchýlka, (6) minimum, (7) maximum, (8) počet

**Table 3** Basic statistic of the values of "*h*" in 2010

| Parameter *h* (1) | CTF field (2) | Control field (3) |
|---|---|---|
| Mean in cm (4) | 1.09 | 1.108 |
| Standard deviation in cm (5) | 0.02 | 0.014 |
| Minimum in cm (6) | 1.06 | 1.072 |
| Maximum in cm (7) | 1.15 | 1.135 |
| Count (8) | 19 | 20 |

**Tabuľka 3** Popisná štatistika parametra "*h*" pre rok 2010
(1) parameter, (2) CTF parcela, (3) kontrolná parcela, (4) priemer, (5) smerodajná odchýlka, (6) minimum, (7) maximum, (8) počet

**Table 4** Basic statistic of the values of "*h*" in 2011

| Parameter *h* (1) | CTF field (2) | Control field (3) |
|---|---|---|
| Mean in cm (4) | 1.123 | 1.114 |
| Standard deviation in cm (5) | 0.020 | 0.009 |
| Minimum in cm (6) | 1.083 | 1.101 |
| Maximum in cm (7) | 1.151 | 1.138 |
| Count (8) | 18 | 18 |

**Tabuľka 4** Popisná štatistika parametra "*h*" pre rok 2011
(1) parameter, (2) CTF parcela, (3) kontrolná parcela, (4) priemer, (5) smerodajná odchýlka, (6) minimum, (7) maximum, (8) počet

For each year, the two data sets were analysed using the F test firstly. In all cases, the test showed that variances of the two datasets were equal. Therefore, the *t*-test: Two Sample assuming Equal Variances was applied. The results are shown in Table 5.

**Table 5** Results of the *t*-test for the three monitored years

| Parameter (1) | 2009 | 2010 | 2011 |
|---|---|---|---|
| t Stat (2) | 1.33 | -2.04 | 1.67 |
| P value (3) | 0.189 | 0.048 | 0.11 |
| t critical (4) | 2.00 | 2.02 | 2.03 |

**Tabuľka 5** Výsledky *t*-testu pre tri sledované roky
(1) parameter, (2) t štatistické, (3) P hodnota, (4) t kritické

For the level of significance $\alpha = 0.05$ it can be concluded that there is no significant difference between the means of the two datasets in 2009 ($t_{stat} = 1.33$, $t_{krit} = 2.00$, $t_{sta} < t_{krit}$). Based on the statistics, there is statistically significant difference ($t_{sta} > t_{krit}$) in 2010, which reaches the value of 0.018 m. However, this difference is negligible from practical point of view. The *t*-test assuming Equal Variances applied for the data of 2011 showed that the difference is not statistically different ($t_{sta} < t_{krit}$).

Soil roughness was assessed through the coefficient of variation (CV) as well. The calculated values are given in Table 6.

**Table 6** The coefficient of variation (CV) for the three years

| Parameter (1) | 2009 | 2010 | 2011 |
|---|---|---|---|
| CV for CTF (2) | 6.37 | 3.04 | 2.18 |
| CV for random (3) | 4.69 | 2.63 | 2.25 |

**Tabuľka 6** Variačné koeficienty pre sledované obdobie
(1) parameter, (2) variačný koeficient pre CTF parcelu, (3) variačný koeficient pre kontrolnú parcelu

Values of the variation coefficient are within an acceptable range, which is confirmed by results of Garcia Moreno et al. (2007). The authors published values of the coefficient of variation ranging from 7.8 % to 14.6 % when comparing different tillage systems.

Based on the results shown in Tables 5 and 6, it can be concluded that the direction of disc harrows movement during the field operation stubble tillage did not have a negative effect on the soil surface roughness after the first CTF growing season.

Similar results were obtained by Hůla et al. (2011), which confirmed that the CTF system did not cause any problems with crop establishment despite the fact that the angle-wise pattern of the tillage operation was not used.

### Conclusion

The three-year study of soil roughness under the controlled traffic system showed that the difference between the CTF and control field was not significant from statistical as well as practical point of view. Soil roughness expressed through the coefficient of variation was in an acceptable range at both fields. Therefore, it can be concluded that the CTF did not cause any problems in terms of the quality of the soil surface.

## Súhrn

Riadený pohyb strojov po poli je technológia, ktorá minimalizuje utlačenú plochu poľa na minimum zavedením tzv. permanentných koľají. V súčasnosti sa spája predovšetkým s minimalizačnými technológiami. Zatiaľ však nie sú známe výsledky o vplyve tejto technológie na vyrovnanosť povrchu pôdy. Systém CTF bol implementovaný na 16 ha parcele, pričom počas 3 rokov bola hodnotená vyrovnanosť povrchu poľa. Každoročne boli hodnoty z experimentálnej CTF parcely porovnané s kontrolnou parcelou. Na základe výsledkov je možné konštatovať, že zavedenie systému CTF nepôsobilo na vyrovnanosť povrchu v negatívnom smere. Vyrovnanosť povrchu nebola štatisticky významne odlišná od kontrolnej parcely s výnimkou jedného roka, kde rozdiel predstavoval 0,018 m, čo je možné z praktického hľadiska považovať za zanedbateľné. Variačný koeficient sa pohyboval v akceptovateľnom rozsahu, 2,18 – 6,37 % pre CTF parcelu a 2,25 až 4,69 % pre kontrolnú parcelu.

**Kľúčové slová:** riadený pohyb strojov po poli, obrábanie pôdy, vyrovnanosť povrchu

### Acknowledgements

This paper was prepared in the frame of the research project funded from the European Union under the title ITEPAg: Application of information technologies to increase the environmental and economic efficiency of the production agro-system. ITMS 26220220014

## References

ANKEN, T. – HOLPP, M. 2007. Controlled traffic farming under Central Europe conditions. [online]. [cit.2012.04.08.]. Available at: http://www.agroscope.admin.ch/data/publikationen/1285328760_Holpp_M_Controlled_REF372.pdf

CHAMEN, W.C.T. 2007. Controlled traffic farming as a complementary practice to no-tillage. In: No-tillage seeding in conservation agriculture. Wallingford : UK.

GALAMBOŠOVÁ, J. et al. 2010. Controlled traffic farming and minimum tillage: results of initial experiments and layout of a long term experiment. In XVIIth World Congress of the International Commission of Agricultural and Biosystems Engineering (CIGR) Available at: <https://www.bioeng.ca/publications/meetings-papers?sobi2Task=sobi2Details&sobi2Id=494>.

GARCIA MORENO, R. et al. 2007. Tillage and soil type effects on soil surface roughness at semiarid climatic conditions. [online]. Available at: http://oa.upm.es/2510/2/INVE_MEM_2008_56620.pdf

GARCIA MORENO, R. et al. 2008. Multifractal analysis of soil surface roughness. [online] Available at: http://oa.upm.es/2510/2/INVE_MEM_2008_56620.pdf

HŮLA, J. a i. Výzkum technologie řízených přejezdů po pozemcích. In Mechanizace zemědělství. Praha : Profi Press s.r.o., roč. 61, 2011, č. 8, s. 46 – 50. ISSN 0373-6776.

KROULIK, 2009. Hodnocení intensity zatíženi půdy pneumatikami zemědělských strojů. Assessment of soil stress intensity under the agricultural machinery tyres. In: GPS autopilot in agriculture, scientific conference, Prague: Czech University of Life Sciences, 2009. ISBN 978-80-213-1993-6

MAYER, V. a i. 2010. Zařízení pro měření stavu povrchu půdy a porostu na půdách. [online]. Available at: http://212.71.135.254/vuzt/vyzkum/2004/mayer1.htm?menuid =120

YULE, D. F. 2006. On-Farm R & D for Controlled Traffic Farming. 2006. In: Sustainability – its impact on soil management and environment: ISTRO 2006

Contact address:
Ing. Jana Galambošová, PhD., prof. Ing. Vladimír Rataj, PhD., Department of Machines and Production Systems, Faculty of Engineering, Slovak University of Agriculture in Nitra, Tr. Andreja Hlinku 2, 949 76 Nitra, Slovakia

Acta technologica agriculturae 1
Nitra, Slovaca Universitas Agriculturae Nitriae, 2012, p. 41–45

# PROTOTYPE OF A GLASS-ROD WAVEGUIDE FOR MONITORING OF BEER FERMENTATION PROCESS USING ACOUSTIC EMISSION

# PROTOTYP SKLENĚNÉHO VLNOVODU PRO MONITOROVÁNÍ PROCESU KVAŠENÍ PIVA MĚŘENÍM AKUSTICKÉ EMISE

David VARNER, Michal ČERNÝ, Jan MAREČEK, Josef LOS

Mendel University, Brno, Czech Republic

The paper presents results of a preliminary experiment focused on usage of a glass-rod waveguide for acoustic emission (AE) monitoring. Acoustic emission was previously used to monitor the fermentation process in the hopped wort. We learned that it was necessary to develop a more effective way of sensor coupling within the fermentation tank. A glass-rod solution was used for direct contact with the hopped wort and this setup was subject to laboratory testing. The first study compared two AE analyser slots with different frequency responses. Optimised waveguide design will be used in the next phase of the fermentation monitoring project.

**Keywords:** beer, fermentation, tank, cylindroconical fermenter, acoustic emission

In 2010, our research team presented results of the first phase of the research project in the Destila micro-brewery. The innovative concept was focused on usage of the acoustic emission (AE) method for monitoring the beer fermentation process. However, after series of testing, it became clear that a different approach had to be chosen. In the original setup, AE sensors were found ineffective when placed on several positions on the cylindroconical fermenter (CCT) body. This might have been due to a complicated tank structure and material used. In this paper, authors further elaborated the method and presented a refined waveguide solution (Varner et al., 2010).

### Beer fermentation basics

Fermentation is a process by which fermentable carbohydrates are converted by yeast into alcohol, carbon dioxide, and numerous other by-products. It is these by-products that have a considerable effect on the taste, aroma, and other properties that characterise the style of beer (Beer Fermentation, 2010).

Cylindroconical fermenters represent common fermentation systems used today to produce both lagers and ales. As the name implies, the enclosed vessels are vertical cylinders with a conical base and, normally, a dished top. This design allows for easy yeast collection and CIP cleaning. They range in size between 100 and 7,000 hl, have from a 1 : 5 to a 3 : 1 ratio of height to diameter, and work under pressures from 1 to 1.3 bars above atmospheric pressure. In fermentation vessels with a ratio greater than 3:1, there is a tendency for increased production of higher alcohols at the expense of esters. Vessel geometry plays an important role in fermentation. As the height-to-diameter ratio increases, so does the mixing of yeast and wort, as well as the fermentation rate (Beer Fermentation, 2010).

### Acoustic emission method

Acoustic emissions are stress waves produced by a sudden internal stress redistribution of materials caused by changes in the internal structure. Possible causes of internal-structure changes are crack initiation and growth, crack opening and closure, dislocation movement, twinning, and phase transformation in monolithic materials and fibre breakage and fibre-matrix debonding in composites. Most of the sources of AE are damage-related; thus, the detection and monitoring of these emissions are commonly used to predict material failure. In technical diagnostics, the AE method has been used to monitor the rotational part status (friction and cavitation of bearings/gears), detection of micro-cracks, pressure vessel defects, tubing system defects, aircraft structure evaluation/testing, and bridge status diagnostics. The AE technique has proven useful in fatigue testing and destruction experiments. Major advantages of AE include continuous monitoring of the object, time savings, and forecast abilities of the concept. On the other hand, the AE wave source is not always obvious as the emitted energy may result from several phenomena inside of the part. Further variable factors include the shape of the object, surface area, material structure, and homogeneity level (Kreidl a Šmíd, 2006).

## Material and methods

### Destila micro-brewery

In Mendel University, there is a Destila micro-brewery in the food production laboratory of the Department of Agriculture, Food and Environmental Engineering. The Destila system serves for model and/or analysis purposes. It allows for amount modifications of malt, hops, yeasts, and other ingredients. Temperature can be streamlined within the actual brewing process as well. The variable configuration features make the micro-brewery an ideal ground for various research projects. Figure 1 shows the fermentation section of the micro-brewery.

The Destila micro-brewery consists of the following main components: mash tun, cooling system, open fermentation tank, storage tank, cylindroconical fermenter, filtration/racking tank, and accessory (electric, boiler, cooling system, and filtration).

In this experiment, the beer fermentation process in the cylindroconical fermenter tank has been subject to AE monitoring. This device allows for a combined and streamlined fermentation process as opposed to primary fermentation in open fermentation tank and secondary fermentation in the storage tank. The cylindroconical fermenter body is made from Cr/Ni stainless steel.

**Figure 1** Cylindroconical fermenter in the Destila micro-brewery. Note the observation opening on top surface
Photo: by David Varner
**Obrázek 1** Cylindrokonický kvasný tank v mikropivovaru Destila
Foto: David Varner

## Glass-rod waveguide solution

For current phase of the research, a glass-rod waveguide set was designed. This feature included an entire new tank accessory assembly. There are two openings in the top of the CCT. These serve for observation purposes as the lids include glass inserts that allow for watching the level and appearance of the hopped wort inside the tank. A small lamp is fixed to one of the openings to make observations easier. In this research, the original glass in the lid assembly will be replaced with a transparent polyurethane plate with opening in the centre. This opening was designed to host the glass-rod waveguide. The 12 mm diameter glass-rod will be fixed in the opening by a flexible glue-like substance that will provide acoustic isolation as well. Figure 2 shows the original status of the opening and glass see-through lid.

This preliminary study was supposed to address three essential issues:

- Overall ability of the system to capture the AE signal through the glass-rod waveguide.
- Selection of the AE analyser slot for optimal AE measurement performance.
- Possible influence of a different immersion rate of the glass-rod waveguide.

While the first two issues were quite straightforward, the third one was closely connected with real life conditions in the beer fermentation tank. During the fermentation process, the hopped wort level does not remain the same as the liquid is drained out for beer quality check purposes. Also, the yeast is being removed from the tank to streamline the fermentation process. It is clear that changes in the immersed portion of the waveguide might affect the resulting data. Thus, it was crucial to determine whether variations of the immersion zone length were likely to affect the AE data properties.

## Experiment description

In order to properly solve the issues listed above, a simple setup was designed in laboratory conditions. A common 800 ml laboratory glass beaker was equipped with a polystyrene lid with two openings, one for a testing glass-rod waveguide (300 mm long, 12 mm in diameter) and one for the conical water filler. A single piezoelectric sensor of appropriate size was glued on one end of the glass rod to capture waves coming from the beaker along the glass rod. Then, a common sparkling water was poured through the filler into the beaker to simulate bubble behaviour of the hopped wort. During this pouring, AE was monitored. Figure 3 shows the glass-rod waveguide with the AE sensor attached to its end.

The distance of the waveguide tip from the beaker bottom was 2 cm. The acoustic response from the bubble development and bursting was monitored for 3 different water levels, i.e. different immersion grades. Each AE measurement run was

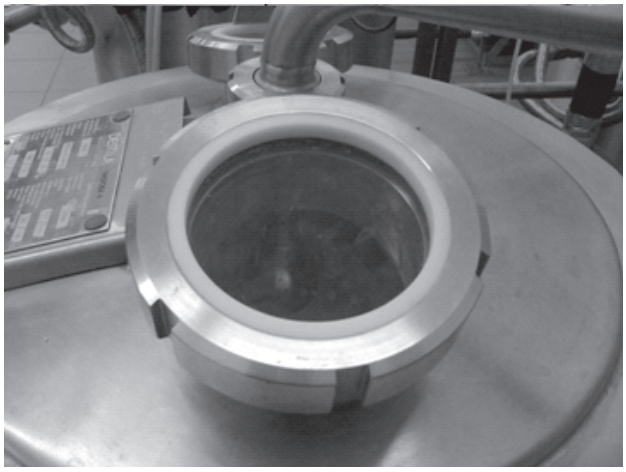

**Figure 2** Opening on the tank body with the original glass lid. A new glass-rod waveguide assembly will be inserted instead of the glass
Photo: by David Varner
**Obrázek 2** Otvor v kvasném tanku s původním skleněným průhledem
Foto: David Varner

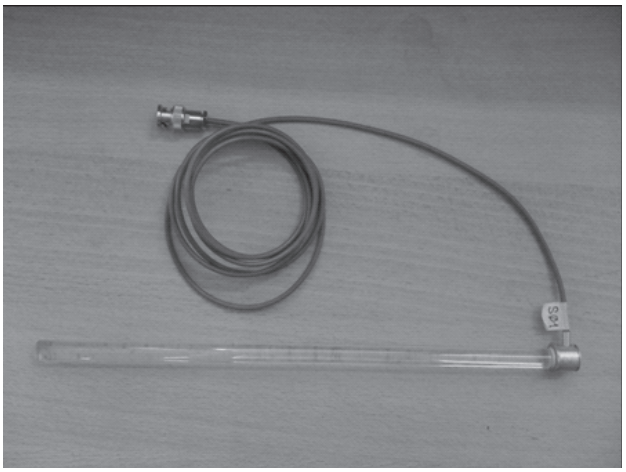

**Figure 3** Testing glass-rod waveguide with piezoelectric AE sensor attached
Photo: by David Varner
**Obrázek 3** Zkušební skleněný vlnovod se snímačem AE
Foto: David Varner

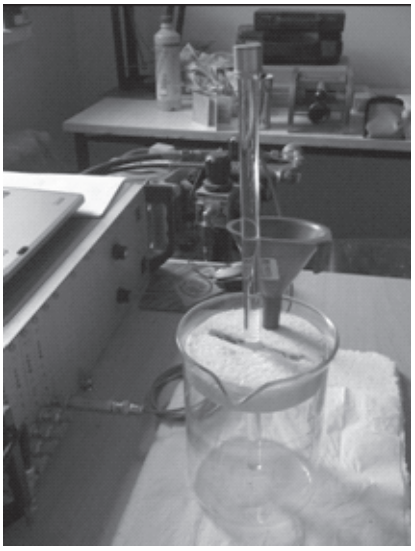

**Figure 4** Testing glass-rod waveguide immersed in the water. Note the blue filler inserted in the polystyrene lid
Photo: by David Varner
**Obrázek 4** Zkušební skleněný vlnovod ponořený ve vodě
Foto: David Varner

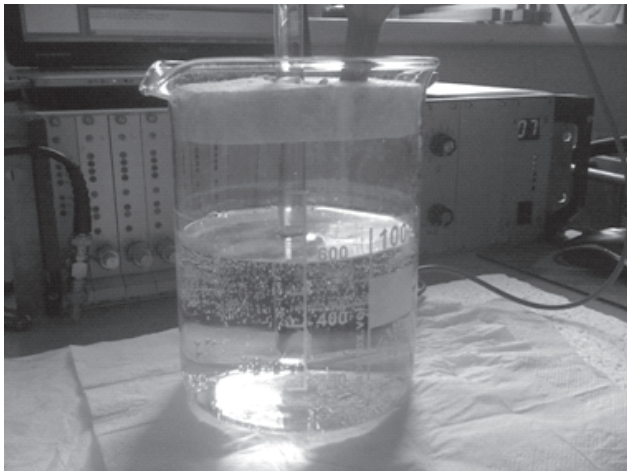

**Figure 5** Detail of the testing glass-rod waveguide. Note the bubbles on the beaker bottom and walls
Photo: by David Varner
**Obrázek 5** Detail zkušebního vlnovodu
Foto: David Varner

10 minutes long. Between each consecutive runs 5 – 7 minute intervals were applied. The actual measurement was initiated after pouring the water and about a 30 second wait time. The reason for this was to eliminate the influence of turbulent flow environment following the pouring.

During the stages, the obvious bubble behaviour was observed including bubble development on the beaker inner surface, gradual growth and finally detachment from walls and bottom. After a vertical upward motion, the bubbles hit the water line, causing severe acoustic impulses registered by the sensor on the waveguide. The entire AE measurement was repeated using two different AE analyser slots: standard slot for 80 – 400 kHz range and updated low frequency slot covering 10 – 200 kHz range. The reason for this procedure was to determine an optimal setup for an effective AE signal reception. The table below lists individual measurement stages together with the corresponding times of measurement.

**Table 1** Overview of the AE analyser slots, water volume in the beaker, immersion zone lengths, and times of measurement

| AE analyser slot type (1) | Water volume in ml (2) | Immersion zone length in cm (3) | Time of measurement (4) |
|---|---|---|---|
| Low frequency (5) | 400 | 3 | 11:11 – 11:21 |
| Low frequency (5) | 600 | 5 | 11:24 – 11:34 |
| Low frequency (5) | 800 | 7 | 11:39 – 11:49 |
| High frequency (6) | 400 | 3 | 13:00 – 13:10 |
| High frequency (6) | 600 | 5 | 13:15 – 13:25 |
| High frequency (6) | 800 | 7 | 13:30 – 13:40 |

**Tabulka 1** Přehled nastavení analyzátoru AE, objemů vody v kádince, hloubek ponoření a časů měření
(1) přehled nastavení analyzátoru AE, (2) objemů vody v kádince, (3) hloubek ponoření, (4) a časů měření

In order to minimise the influence of ambient environment, 50 Ohm terminators were used on the remaining four channels of the AE analyser. There is a salt corrosion chamber in the adjacent room that might affect the measurement due to severe electromagnetic pulses generated by the salt mist generator switch. During the test, the following significant AE signal parameters have been taken into account:

- RMS (Root Mean Square) indicates the so called „effective" value or „energy" of the signal. RMS indicates quantity properties of acoustic emission events. RMS is measured in Volts. In this experiment, RMS indicated the perceptivity of the AE analyser slot.
- A C2 count rate indicates the amplitude range of the signal as it registers crossings of the set threshold level. For this experiment, the C1 (lower level) was left out the evaluation. The C2 count was used to illustrate the rate more clearly.
- PSD (Power Spectral Density) function maximum values of the AE events indicate the distribution of energy transmitted over the frequency spectrum (similar to FFT showing the amplitudes over frequency domain). PSD graphs show one or more peaks. Transformation of the signal to frequency domain was done using the Hanning window. PSD is measured in mW/Hz or dBm/Hz for the logarithmic scale. See the charts at the end of the paper for more information.
- The Dakel XEDO AE analyser was used in the experiment. Most configuration values were left on default settings, as listed in Table 2.

**Table 2** Dakel XEDO AE analyser configuration used uniformly during the experiment

| AE Parameter (1) | Value (2) |
|---|---|
| Sampling frequency (3) | 4 MHz |
| Gain (analyser) (4) | |
| Gain (pre-amplifier) (5) | |
| Maximum Range (6) | |
| AE Event Start Threshold (7) | |
| AE Event End Threshold (8) | |
| C1 Count Threshold (9) | |
| C2 Count Threshold (10) | |

**Tabulka 2** Nastavení analyzátoru Dakel XEDO AE
(1) parametry AE, (2) hodnoty, (3), vzorkovací frekvence, (4) zisk analyzátoru, (5), zisk předzesilovače, (6) maximální rozsah, (7) práh začátku události, (8) práh konce události, (9) práh překmitů C1, (10) práh překmitů C2

## Results and discussion

Two AE slots were used in the experiment with different immersion zones lengths and water volumes. For each slot, the AE record was analysed to find the optimal setup for real monitoring in the Destila micro-brewery conditions. The sensor used was the same for both slots.

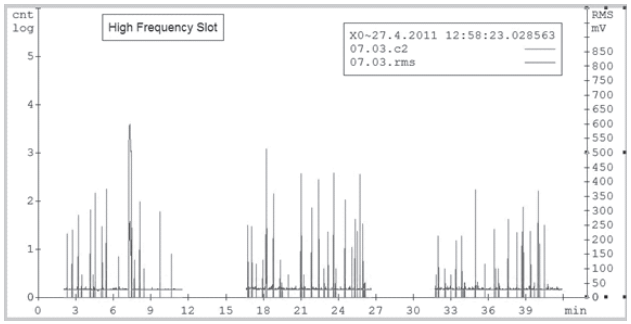


**Figure 6** Chart of RMS and C2 values for standard AE analyser slot. Note the three measurement stages and wait-times intervals
**Obrázek 6** Graf RMS a překmitů C2 pro standardní desku analyzátoru AE

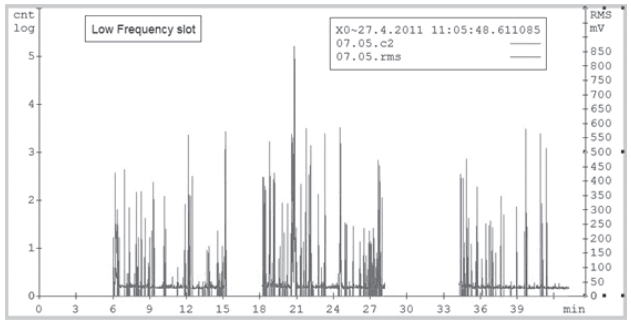


**Figure 7** Chart of RMS and C2 values for updated low frequency AE analyser slot
**Obrázek 7** Graf RMS a překmitů C2 pro nízkofrekvenční desku analyzátoru AE

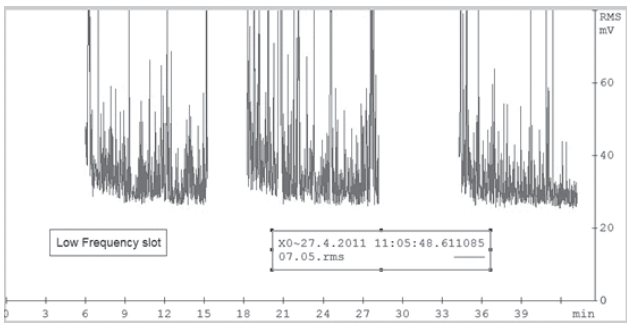


**Figure 8** Detail of the RMS record for low frequency AE analyser slot. Note the decreasing trend in each measurement stage
**Obrázek 8** Detail záznamu RMS pro nízkofrekvenční desku analyzátoru AE

As can be clearly seen in the AE charts below, each AE analyser slot showed a different response to the AE signal. The charts show RMS values in blue and C2 counts in red. Note that the charts have the same axis settings so that the values are visually comparable.

The charts prove that the standard AE analyser slot has much weaker response to the bubble-emitted signal than the updated low frequency slot.

In detail, we can see even a slight decreasing trend at the beginning of each measurement phase. This is obviously due to the settling activity of bubbles after initial turbulent flow conditions.

As far as the PSD function maximum values are concerned, there are several types of AE events. However, a detailed signal sample analysis is beyond the extent of this paper. Four significant types of AE events could be identified in the entire dataset. These probably correspond to different modes of bubble disintegration. Below you can see the AE event samples and associated PSD function peaks. The amplitude on the left is in mV, while the X-axis on the right represents frequency domain in kHz.

Based on the presented results, a real waveguide will be manufactured. This completely new design will include a clear perspex (plexiglas) disc precisely sized according to glass insert in the CCT observation openings. There will be a hole in the disc centre accommodating the actual glass rod waveguide. Notches on the glass rod are going to indicate various immersion zones.

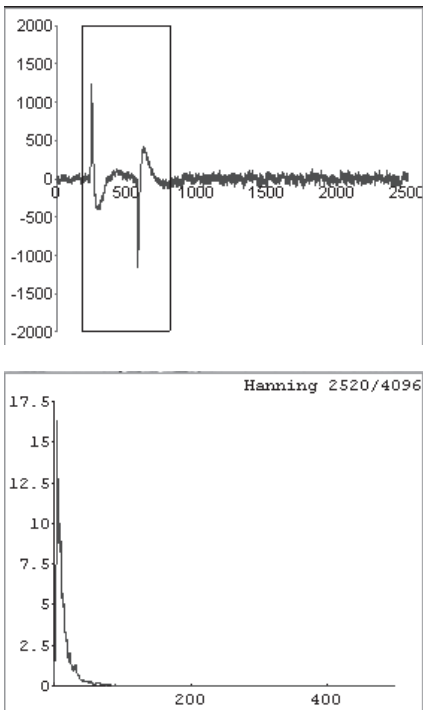


**Figure 9a** Four significant types of AE events obtained during the experiment. Note the Hanning selection window on the sample and corresponding PSD of the signal portion
**Obrázek 9a** Čtyři typické ukázky událostí AE získané během experimentu

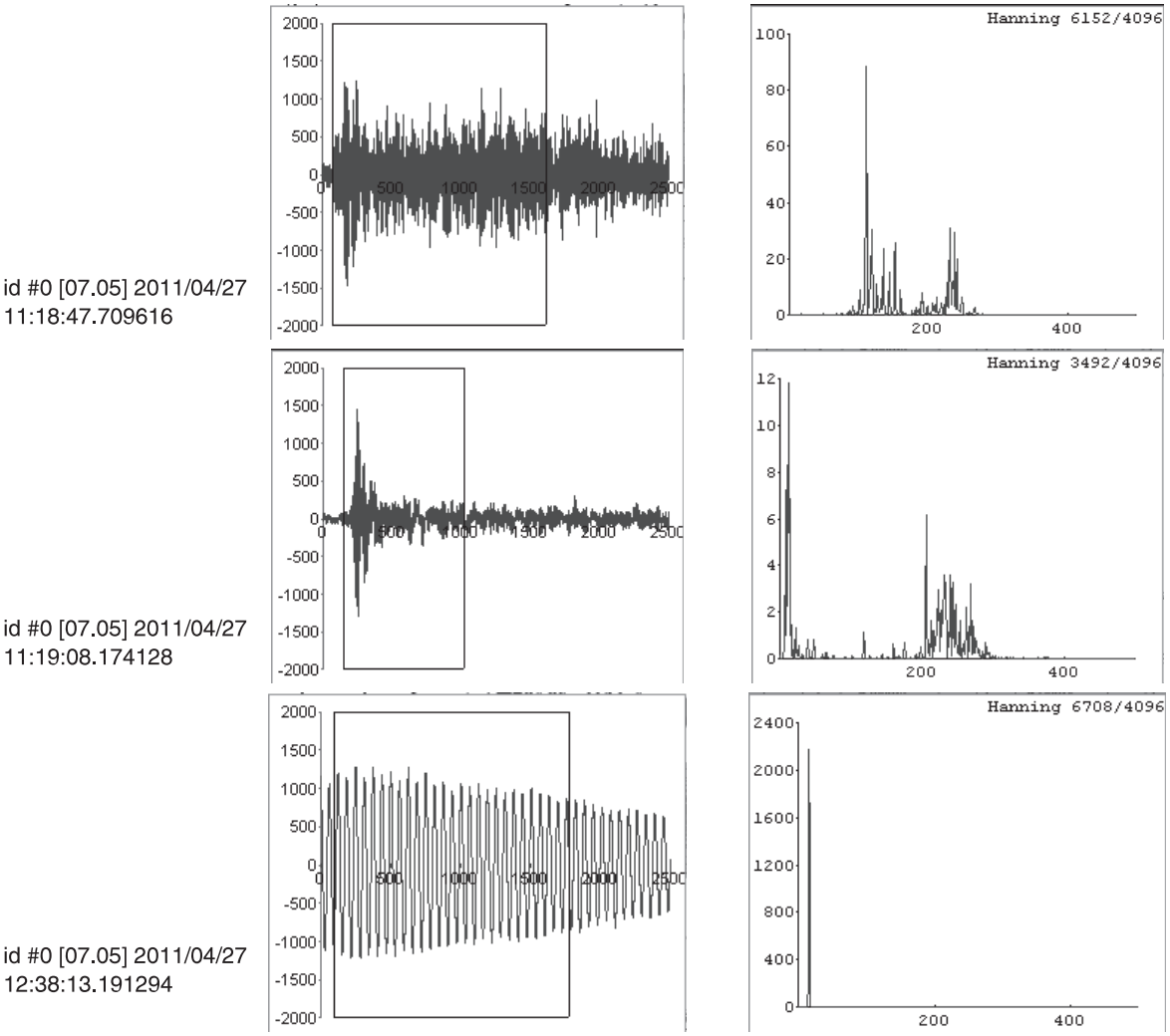


**Figure 9b** Four significant types of AE events obtained during the experiment. Note the Hanning selection window on the sample and corresponding PSD of the signal portion

**Obrázek 9b** Čtyři typické ukázky událostí AE získané během experimentu

## Conclusion

The experiment revealed several interesting facts concerning the usability of the glass-rod waveguide. Based on the signal reception level, low frequency AE analyser slot was chosen for the optimum performance of the system. Three different immersion levels were examined for the waveguide. It can be presumed that changes of the hopped wort volume will have no significant effect on the waveguide functionality. Further testing will be performed in real Destila micro-brewery with a real hopped wort batch and updated waveguide assembly inserted into the tank body.

## Souhrn

Článek popisuje výsledky pilotního experimentu zaměřeného na testování použitelnosti skleněného vlnovodu při měření akustické emise (AE). Na základě výsledků předchozích měření AE bylo nutné vyvinout nový způsob umístění snímačů AE za účelem dosažení lepšího akustického kontaktu s probíhajícím procesem. Jako vhodný materiál byla zvolena skleněná tyč, která bude umístěna do cylindrokonického tanku (CCT) a bude v přímém kontaktu s mladinou. Tyč byla testována v laboratorních podmínkách s dvěma různými sloty analyzátoru AE. Výsledky tohoto experimentu budou využity při výrobě skutečné sestavy vlnovodu pro mikro-pivovar Destila.

**Klíčová slova:** pivo, kvašení, tank, cylindrokonický tank, akustická emise

## References

BEER FERMENTATION [online]. Available from www: <http://www.beer-brewing.com> [quot. 2010-09-26].

KREIDL, M. – ŠMÍD, R. 2006. Technická diagnostika (Technical Diagnostics). 1. vyd. Praha : Nakladatelství BEN, 2006

MONITORING OF BEER Fermentation Process Using Acoustic Emission Method. In MendelNet 2010 Proceedings of International Ph.D. Students Conference. 1. vyd. Brno : Mendelova univerzita, 2010, s. 651 – 659. ISBN 978-80-7375-453-2.

Contact address:
Mgr. David Varner, Department of Engineering and Automobile Transport, Faculty of Agronomy, Mendel University, Brno, Czech Republic, e-mail: info@davar.cz

Acta technologica agriculturae 2
Nitra, Slovaca Universitas Agriculturae Nitriae, 2012, p. 46–52

# MATHEMATICAL MODEL OF A SLIDING COUPLE LUBRICATED WITH BIOLUBRICANTS

# MATEMATICKÝ MODEL KLZNEJ DVOJICE MAZANÝ BIOMAZIVOM

Jozef RÉDL, Veronika VÁLIKOVÁ, Michal KROČKO

Slovak University of Agriculture in Nitra, Slovak Republic

In this paper, we deal with a mathematical analysis of the rotor – sliding bearing system which is lubricated with different types of biolubricants and with the stability simulation of a shaft motion in the sliding bearing. The stability of the rotating shaft was described with the system of differential equations and solved numerically. For simplifying the mathematical description we used the Sommerfeld number to define physical properties of each biolubricant used. To determine the Sommerfeld number we used technical parameters of the oils MOL Traktol NH Ultra and MOL Farm UTTO Synt. The loading cycle during simulation was determined in the range of 200 – 1000 N. The material of the shaft was hardened and tempered steel 12 050. The sliding bearing that we used was B30/38x30 STN 02 3496. We solved the trajectory and stability condition for each type of biolubricant and for the rotating shaft, too. Simulations were made at the temperature of 40 – 100 °C. Properties of both examined biolubricants have almost the same influence on the stability of the shaft moving in the bearing. Stiffness and damping properties of both oils are comparable.

**Keywords:** mathematical modelling, slide bearing, biolubricants

In many mechanical applications, there are very often used slide bearing systems, except for agricultural machines. Because of frequent accidents at a working place, ground contamination with liquid lubricants is very probable. For these reasons, constructions of rotating components and systems make an effort to lubricate with biolubricants that are not biologically dangerous, but they are environmentally friendly decomposable organic matters. Naturally, biolubricants have different physical properties in comparison with petroleum-based oils and lubricants. That is why we are dealing with modelling the effect of biolubricants on rotor stability in the slide bearing.

The mathematical description of rotor dynamics assembled in the slide bearing was published by many authors. Among the most known authors belong Gasch and Pfützner (1975) who mathematically described damped and undamped Laval rotor on rigid bearings. There is also defined the Laval rotor with inside and outside damping. There are shown differential equations for the rotor assembled in the slide bearing and stability criteria of the rotor assembled in the slide bearing, as well as the influence of gyroscopic effect on the stability of a rotating shaft, too. In the mathematical description, the authors used a constant called the Sommerfeld number to define physical properties of lubricants.

An analytical and numerical approach of the slide bearing lubricated surface was investigated by Malvano et al. (1999). An important work of rotor dynamics was published by Genta (2005). The effect of bearing cage run-out on the non linear dynamics of the rotating shaft was analysed by Nataraj and Harsha (2008).

## Material and methods

For simulation we have chosen a radial slide bearing, the parameters of which are described in Table 1. The slide bearing will be loaded by static force $F = 1\,000$ N. The nominal diameter of the bearing is $d = 30{\cdot}10^{-3}$ m and its material is constructional steel with the modulus of elasticity $E = 2.1{\cdot}10^{5}$ MPa. The material of the cage is CuSn alloy with the modulus of elasticity $E_p = 1.1{\cdot}10^{5}$ MPa, and the material of the bearing body is constructional steel with the modulus of elasticity $E_L = 2.1{\cdot}10^{5}$ MPa. The rotational speed of the shaft is $n = 1\,430$ min$^{-1}$, the fit of the cage and bearing body is H7/r6.

**Table 1** Technical parameters of the bearing

| Parameter (1) | Description (2) | Unit (3) | Value (4) |
|---|---|---|---|
| Bearing type (5) | | | Bearing B30/38 × 30 STN 02 3496 |
| B | bearing width (6) | m | 0.030 |
| D | diameter of bearing (7) | m | 0.038 |
| d | diameter of journal (8) | m | 0.030 |

**Tabuľka 1** Technické parametre ložiska
(1) parameter, (2) popis, (3) jednotka, (4) hodnota, (5) typ ložiska, (6) šírka ložiska, (7) priemer ložiska (puzdra), (8) priemer čapu

The slide bearing is lubricated with two types of universal biolubricants, mostly used as gearbox lubricants and for hydraulic circuits used in agricultural tractors. These biolubricants are called Traktol NH Ultra and Farm UTTO Synt. and are manufactured by MOL Hungarian Oil and Gas Company Plc. The basic parameters of oils are shown in Table 2.

### Definition of the initial condition parameters

To prepare a solution of basic dimensions of the bearing, we have to define initial conditions. Values of certain conditions must be evaluated from the data defined in Table 1 hereinbefore. To calculate bearing dimensions and parameters, we used the methodology described by Fiala et al. (1989). Angular velocity $\omega = 149.75$ s$^{-1}$, relative height of the bearing $b^* = 1.10^{-3}$ m, initial oil pressure $P_0 = 0.1$ MPa, initial oil temperature $T_o = T_v = 40$ °C, temperature of bearing vicinity $T_u = 20$ °C, radial temperature gradient of the bearing body and

**Table 2** Parameters of oils

| Parameter (1) | Description (2) | Unit (3) | Oil (4) | |
|---|---|---|---|---|
| | | | MOL Traktol NH Ultra | MOL Farm UTTO Synt. |
| $\rho$ | density (5) | $kg.m^{-3}$ | 888 | 868.1 |
| $\nu_{oil(40)}$ | kinematic viscosity at 40 °C (6) | $m^2.s^{-1}$ | $6{\cdot}10^{-5}$ | $5.814{\cdot}10^{-5}$ |
| $\nu_{oil(100)}$ | kinematic viscosity at 100 °C (7) | $m^2.s^{-1}$ | $1.07{\cdot}10^{-5}$ | $1.022{\cdot}10^{-5}$ |
| $\eta_{oil(40)}$ | dynamic viscosity at 40 °C (8) | Pa.s | 0.05328 | 0.050471334 |
| $\eta_{oil(100)}$ | dynamic viscosity at 100 °C (9) | Pa.s | $9.5016{\cdot}10^{-3}$ | $8.871982{\cdot}10^{-5}$ |

**Tabuľka 2** Vlastnosti olejov
(1) parameter, (2) popis, (3) jednotka, (4) olej, (5) hustota, (6) kinematická viskozita pri 40 °C, (7) kinematická viskozita pri 100 °C, (8) dynamická viskozita pri 40 °C, (9) dynamická viskozita pri 100 °C

slide $\Delta T_{rL}$ = 15 °C, radial temperature gradient of the slide and geometrical centre of the shaft $\Delta T_{rH}$ = 5 °C, coefficient of thermal expansion of the bearing body $\alpha_L = 18.4{\cdot}10^{6}$ °C$^{-1}$, coefficient of thermal expansion of the shaft journal $\alpha_H = 11.7{\cdot}10^{6}$ °C$^{-1}$, roughness of the shaft $R_{aH}$ = 0.4 μm, roughness of the cage $R_{aP}$ = 0.8 μm, oil filter mesh value $a$ = 8 μm. Other parameters are solved as follows:

- Circumferential speed $\nu_H$:

$$\nu_H = \pi \cdot d \cdot n = 2.246\ \text{m.s}^{-1} \tag{1}$$

- Bearing hydrodynamic effective clearance $\Psi_e$:

$$\Psi_e = 0.8 \cdot 10^{-3} \cdot \sqrt[4]{\nu_H} = 0.97936 \cdot 10^{-3} \tag{2}$$

- Bearing acting pressure $P_m$:

$$P_m = \frac{F}{b \cdot d} = 1.111\ \text{MPa} \tag{3}$$

- Cage thickness $s^*$:

$$s^* = 0.9 \cdot d = 2.7 \cdot 10^{-3}\ \text{m} \tag{4}$$

where the condition $s^* < \cdot\, d$ must be satisfied

- Thickness of the bearing lining $s_v$:

$$s_v = 0.03 \cdot d = 0.9 \cdot 10^{-3}\ \text{m} \tag{5}$$

- Diameter of the bearing cage $D_1$:

$$D_1 = d + 2 \cdot s^* = 35.4 \cdot 10^{-3}\ \text{m we chose } D_1 = 38{\cdot}10^{-3}\ \text{m} \tag{6}$$

- Average value of the interference $\Delta D_1$ = 25 μm, with respect to the tolerance of steel on the bronze rod end of the inner ring.
- Relative interference $\vartheta$:

$$\vartheta = \frac{\Delta D_1}{D_1} = 0.65789 \cdot 10^{-3} \tag{7}$$

- Diameter of the bearing $D_2$:

$$D_2 = 1.5 \cdot D_1 = 57 \cdot 10^{-3}\ \text{m} \tag{8}$$

- Coupling constant for the bearing $C_L$:

$$C_L = \frac{\left(\frac{D_2}{D_1}\right)^2 + 1}{\left(\frac{D_2}{D_1}\right)^2 - 1} = 2.6 \tag{9}$$

- Coupling constant for the bearing cage $C_P$:

$$C_P = \frac{\left(\frac{D_1}{d}\right)^2 + 1}{\left(\frac{D_1}{d}\right)^2 - 1} = 4.309 \tag{10}$$

- Contact pressure $P_1$:

$$P_1 = \partial \frac{E_L \cdot E_P}{E_P(C_L + \nu_L) + E_L(C_P + \nu_P)} = 13.21\ \text{MPa} \tag{11}$$

- Change of the bearing clearance due to forcing-in of the cage $\Delta d_P$:

$$\Delta d_P = -\frac{P_1 \cdot d}{E_P}\left[\frac{2}{1 - \left(\frac{d}{D_1}\right)^2}\right] = -0.019{\cdot}10^{-3}\ \text{m} \tag{12}$$

- Effective height of the bearing cage $s$:

$$s = \left[\frac{(D_1 - d)}{2}\right] - \frac{s_v}{2} = 3.55 \cdot 10^{-3}\ \text{m} \tag{13}$$

- Change factor of the relative interference $B$:

$$B = \frac{\frac{4 \cdot s \cdot E_P}{D_1}\left(1 - \frac{s}{D_1}\right) \cdot}{\frac{4 \cdot s \cdot E_P}{D_1}\left(1 - \frac{s}{D_1}\right)\left[1 - \nu_L + (1 + \nu_V)\left(\frac{D_2}{D_1}\right)^2\right] + \cdot\left[1 - \nu_L + (1 + \nu_V)\left(\frac{D_2}{D_1}\right)^2\right]}{E_L\left[\left(\frac{D_2}{D_1}\right)^2 - 1\right]\left[1 - \nu_P + (1 + \nu_P)\left(1 - \frac{2s}{D_1}\right)^2\right]} = 0.25 \tag{14}$$

- Change of the relative bearing clearance $\Delta\Psi_T$,

$$\Delta\Psi_T = (\alpha_L - \alpha_H)(1 - B)(T_v - T_u) - \\ -0.6(\alpha_L \cdot \Delta T_{rL} - 0.75 \cdot \alpha_H \cdot \Delta T_{rH}) = -1.292{\cdot}10^{-3} \tag{15}$$

- Average diameter of the bearing cage $\overline{D}$ = 30.021·10$^{-3}$ m, corresponding with the coupling $\phi$ 30*H7*, according to ISO 12240-1.
- Average diameter of the shaft $\overline{d}_{av}$:

$$\overline{d}_{av} = \overline{D} - \Psi_e \cdot +6.8(R_{aH} + R_{aP}) + \\ +\Delta d_P + \Delta\Psi_T \cdot d = 29.9422 \cdot 10^{-3}\ \text{m} \tag{16}$$

- Real average diameter of the shaft $\overline{d}$, with respect to variance from the nominal diameter of the shaft and defined tolerance zone, it will be $\overline{d}$ = 29.8812·10$^{-3}$ m.
- Average relative bearing clearance $\overline{\Psi}_e$:

$$\overline{\Psi}_e = \frac{\left[\overline{D} - d + 6.8(R_{\alpha H} + R_{\alpha P}) + \Delta d_P\right]}{d} + \Delta\Psi_T = 3.003 \cdot 10^{-3} \quad (17)$$

- Minimum oil film thickness $h_0$:

$$h_0 = 3.4(R_{\alpha H} + R_{\alpha P}) + \alpha = 0.01208 \cdot 10^{-3} \text{ m} \quad (18)$$

- Relative eccentricity ε:

$$\varepsilon = 1 - \left(\frac{2 \cdot h_0}{\overline{D} - \overline{d}}\right) = 0.82718 \quad (19)$$

with respect to the condition ε > 0.7.

- Bearing clearance:

$$C = \frac{\overline{D} - \overline{d}}{2} = 69.9 \cdot 10^{-6} \text{ m} \quad (20)$$

- Real average radius of the shaft:

$$\overline{R} = \frac{\overline{d}}{2} = 14.9406.10^{-3} \text{ m} \quad (21)$$

- Sommerfeld number $S_O$:

$$S_O = \frac{P_m \cdot \overline{\Psi}_e^2}{\eta_T \cdot \omega} \quad (22)$$

with respect to $\frac{b}{d}$ = 1.0, ε = 0.82718. The Sommerfeld numbers for both oils were calculated with respect to the initial temperature of oils and operating temperature of oils or of the bearing. The calculated values are in Table 3.

Stiffness and damping coefficients of the bearing, which are dependent on dynamic viscosity, are solved with Equations 23, 24, published by Wang and Khonsari (2006). The solved parameters are shown in Table 4 and 5.

$$k_{yy} = \frac{\varepsilon\omega\eta\overline{R}L^3}{C^3(1-\varepsilon^2)^2}, \quad k_{yz} = -\frac{\pi\omega\eta\overline{R}L^3(1+2\varepsilon^2)}{4C^3\sqrt{(1-\varepsilon^2)^5}} \quad (23)$$

$$k_{zy} = \frac{\pi\omega\eta\overline{R}L^3}{4C^3\sqrt{(1-\varepsilon^2)^3}}, \quad k_{zz} = \frac{2\omega\eta\overline{R}L^3\varepsilon(1+\varepsilon^2)}{C^3(1-\varepsilon^2)^3}$$

$$c_{yy} = \frac{\pi\eta\overline{R}L^3}{2C^3\sqrt{(1-\varepsilon^2)^3}}, \quad c_{yz} = -\frac{2\varepsilon\eta\overline{R}L^3}{C^3(1-\varepsilon^2)^2} \quad (24)$$

$$c_{zy} = -\frac{2\varepsilon\eta\overline{R}L^3}{C^3(1-\varepsilon^2)^2}, \quad c_{zz} = \frac{\pi\eta\overline{R}L^3(1+2\varepsilon^2)}{2C^3\sqrt{(1-\varepsilon^2)^5}}$$

We solved dimensionless parameters of stiffness and damping by Equations (25) and (26) according to Gomez-Manzilla et al. (2005). Solved parameters are shown in Tables 6 and 7.

$$\gamma_{ij} = \frac{C}{F}k_{ij};\ (i, j = y, z) \quad (25)$$

$$\beta_{ij} = \frac{C \cdot \omega}{F}c_{ij};\ (i, j = y, z) \quad (26)$$

**Table 3** Sommerfeld numbers

| Parameter (1) | Description (2) | Unit (3) | Oil (4) | |
|---|---|---|---|---|
| | | | MOL Traktol NH Ultra | MOL Farm UTTO Synt. |
| $S_{O(40)}$ | sommerfeld numbers (5) | – | 1.253 | 1.3229 |
| $S_{O(100)}$ | | – | 7.0273 | 7.526 |

**Tabuľka 3** Sommerfeldove čísla
(1) parameter, (2) popis, (3) jednotka, (4) olej, (5) Sommerfeldove čísla

**Table 4** Stiffness values of the bearing

| Stiffness (1) ($N \cdot m^{-1}$) | Sommerfeld number (2) | | | |
|---|---|---|---|---|
| | 1,253 | 7,0273 | 1,3229 | 7,526 |
| $k_{yy}$ | 7.8177302·10$^7$ | 1.3941619·10$^7$ | 7.405617·10$^7$ | 1.3017786·10$^7$ |
| $k_{yz}$ | -3.1285834·10$^8$ | -5.579307·10$^7$ | -2.9636595·10$^8$ | -5.2095975·10$^7$ |
| $k_{zy}$ | 4.171173·10$^7$ | 7438591.8675 | 3.9512888·10$^7$ | 6945677.90205 |
| $k_{zz}$ | 8.3394211·10$^8$ | 1.4871968·10$^8$ | 7.8998068·10$^8$ | 1.3886485·10$^8$ |

**Tabuľka 4** Tuhosti ložiska
(1) tuhosť, (2) Sommerfeldovo číslo

**Table 5** Damping values of the bearing

| Damping (1) ($N \cdot s \cdot m^{-1}$) | Sommerfeld number (2) | | | |
|---|---|---|---|---|
| | 1,253 | 7,0273 | 1,3229 | 7,526 |
| $c_{yy}$ | 557 084.876105 | 99 346.8029054 | 527 718.033938 | 92 763.6447687 |
| $c_{yz}$ | -1 044 104.20621 | -186 198.583442 | -989 064.04134 | -173 860.2425619 |
| $c_{zy}$ | -1 044 104.20621 | -186 198.583442 | -989 064.04134 | -173 860.2425619 |
| $c_{zz}$ | 4 178 408.51721 | 745 149.5189041 | 3 958 142.86525 | 695 772.6192458 |

**Tabuľka 5** Tlmenia ložiska
(1) tlmenie, (2) Sommerfeldovo číslo

**Table 6** Dimensionless stiffness coefficients of the bearing

| Stiffness (1) | Sommerfeld number (2) | | | |
|---|---|---|---|---|
| | 1,253 | 7,0273 | 1,3229 | 7,526 |
| $\gamma_{yy}$ | 5.4645934 | 0.9745192 | 5.1765263 | 0.9099432 |
| $\gamma_{yz}$ | -21.8687978 | -3.8999356 | -20.7159797 | -3.6415086 |
| $\gamma_{zy}$ | 2.9156499 | 0.5199576 | 2.7619509 | 0.4855029 |
| $\gamma_{zz}$ | 58.2925535 | 10.3955054 | 55.2196497 | 9.7066533 |

**Tabuľka 6** Bezrozmerné tuhosti ložiska
(1) tuhosť, (2) Sommerfeldovo číslo

**Table 7** Dimensionless damping coefficients of the bearing

| Damping (1) | Sommerfeld number (2) | | | |
|---|---|---|---|---|
| | 1,253 | 7,0273 | 1,3229 | 7,526 |
| $\beta_{yy}$ | 5.8312999 | 1.0399151 | 5.5239017 | 0.9710058 |
| $\beta_{yz}$ | -10.9291869 | -1.9490383 | -10.3530526 | -1.8198864 |
| $\beta_{zy}$ | -10.9291869 | -1.9490383 | -10.3530526 | -1.8198864 |
| $\beta_{zz}$ | 43.7375956 | 7.7998712 | 41.4319594 | 7.2830173 |

**Tabuľka 7** Bezrozmerné tlmenia ložiska
(1) tlmenie, (2) Sommerfeldovo číslo

## Mathematical model

The mathematical model is based on the basic theory of rotor dynamics published by Gasch and Pfützner (1975) and Genta (2005). The model is shown in Figure 1. Stiffness and damping properties of the bearing are simulated with a simple spring-damper model oriented to the y and z coordinate system. In Figure 1, there is defined the minimum oil film thickness which lies on the line of centres. The line of centres is a connecting line of the centre of the shaft and the centre of the bearing. In operating condition, the line of centres changes, and the centre of the shaft performs certain motion, which will be analysed below.

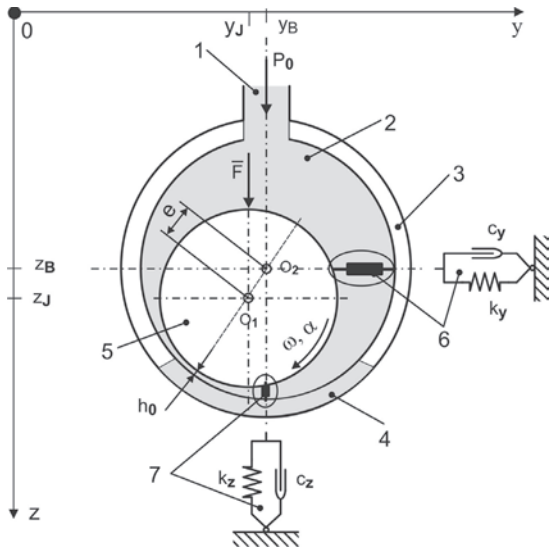


**Figure 1** Mathematical model of the bearing
1 – oil flow with pressure $P_0$, 2 – oil, 3 – bearing, 4 – bearing shell, 5 – shaft, 6 – spring-damper model with respect to the *y* axis, 7 – spring-damper model with respect to the *z* axis

**Obrázok 1** Matematický model ložiska
1 – prívod oleja pod tlakom $P_0$, 2 – olej, 3 – ložisko, 4 – ložisková panva, 5 – hriadeľ, 6 – model pružina – tlmič v osi *y*, 7 – model pružina – tlmič v osi *z*

We suppose a stationary system where angular velocity $\omega$ is constant, angular acceleration is $\alpha = 0$, and the relationship between coordinates of the shaft centre and bearing centre is as follows:

$$z_B = z_J + \varepsilon \cdot \cos\varphi \qquad (27)$$
$$y_B = z_J + \varepsilon \cdot \sin\varphi$$

where:

$\varphi$ – is the angle between the line of centres and the relevant coordinate axis. Script indexes *B* and *J* denote: *B* – bearing and *J* – shaft

Motion equations of the eccentrically positioned shaft in the bearing can be used in the following form:

$$m \cdot \ddot{z}_T = -c_z \cdot \dot{z}_H - k_z \cdot z_H \qquad (28)$$

$$m \cdot \ddot{y}_T = -c_y \cdot \dot{z}_y - k_y \cdot z_y \qquad (29)$$

$$I \cdot \alpha = \varepsilon \cdot (y_J \cdot k_y \cdot \cos\varphi + \dot{y}_J \cdot c_y \cdot \cos\varphi - z_J \cdot k_z \cdot \cos\varphi - \dot{z}_J \cdot c_z \cdot \cos\varphi) + M \qquad (30)$$

where:

*M* – is the couple of forces, *I* is the moment of inertia of the system with respect to the axis of rotation. Combining Equation (27) with Equations (28, 29) gives us the motion equations in the matrix form as follows:

$$\frac{m}{2} \cdot \begin{bmatrix} \ddot{z}_J \\ \ddot{y}_J \end{bmatrix} + \begin{bmatrix} c_{zz} & c_{zy} \\ c_{yz} & c_{yy} \end{bmatrix} \cdot \begin{bmatrix} \dot{z}_J \\ \dot{y}_J \end{bmatrix} + \begin{bmatrix} k_{zz} & k_{zy} \\ k_{yz} & k_{yy} \end{bmatrix} \cdot \begin{bmatrix} z_J \\ y_J \end{bmatrix} = \varepsilon \cdot \omega^2 \cdot \frac{m}{2} \cdot \begin{bmatrix} \cos\omega t \\ \sin\omega t \end{bmatrix} \qquad (31)$$

If we multiply Equation (31) with the parameter $\frac{S_O \cdot C}{F}$ and use Equations (28, 29), we obtain the motion equations in the form:

$$\frac{S_O \cdot C}{g} \cdot \begin{bmatrix} \ddot{z}_J \\ \ddot{y}_J \end{bmatrix} + \frac{1}{\omega} \cdot \begin{bmatrix} \beta_{zz} & \beta_{zy} \\ \beta_{yz} & \beta_{yy} \end{bmatrix} \cdot \begin{bmatrix} \dot{z}_J \\ \dot{y}_J \end{bmatrix} + \begin{bmatrix} \gamma_{zz} & \gamma_{zy} \\ \gamma_{yz} & \gamma_{yy} \end{bmatrix} = \varepsilon \cdot \omega^2 \cdot \frac{S_O \cdot C}{g} \cdot \begin{bmatrix} \cos\omega t \\ \sin\omega t \end{bmatrix} \qquad (32)$$

and finally:

$$\frac{S_O \cdot C}{g} \cdot \begin{bmatrix} \ddot{z}_J \\ \ddot{y}_J \end{bmatrix} + \frac{1}{\omega} \cdot \begin{bmatrix} \beta_{zz} & \beta_{zy} \\ \beta_{yz} & \beta_{yy} \end{bmatrix} \cdot \begin{bmatrix} \dot{z}_J \\ \dot{y}_J \end{bmatrix} + \begin{bmatrix} \gamma_{zz} & \gamma_{zy} \\ \gamma_{yz} & \gamma_{yy} \end{bmatrix} = 0 \quad (33)$$

The stability of the shaft motion in the bearing can be considered by solving the system of homogenous differential equations (33). We will search the solution of this system in the form:

$$\begin{bmatrix} z_{Jo} \\ y_{Jo} \end{bmatrix} = \begin{bmatrix} \hat{z}_{Jo} \\ \hat{y}_{Jo} \end{bmatrix} \cdot e^{\lambda t} \quad (34)$$

If we respect an assumption:

$$\dot{z}_{Jo} = \lambda \cdot \hat{z}_{Jo} \cdot e^{\lambda t}, \quad \ddot{z}_{Jo} = \lambda^2 \cdot \hat{z}_{Jo} \cdot e^{\lambda t} \quad (35)$$
$$\dot{y}_{Jo} = \lambda \cdot \hat{y}_{Jo} \cdot e^{\lambda t}, \quad \ddot{y}_{Jo} = \lambda^2 \cdot \hat{y}_{Jo} \cdot e^{\lambda t}$$

and put Equation (34) into Equation (33), then, after modifying, we get the system of algebraic equations in the form:

$$\left(\frac{S_O \cdot C}{g} \cdot \lambda^2 + \frac{\lambda}{\omega} \cdot \beta_{zz} + \gamma_{zz}\right) \cdot \hat{z}_{Jo} + \left(\frac{\lambda}{\omega} \cdot \beta_{zy} + \gamma_{zy}\right) \cdot \hat{y}_{Jo} = 0 \quad (36)$$
$$\left(\frac{S_O \cdot C}{g} \cdot \lambda^2 + \frac{\lambda}{\omega} \cdot \beta_{yy} + \gamma_{yy}\right) \cdot \hat{y}_{Jo} + \left(\frac{\lambda}{\omega} \cdot \beta_{yz} + \gamma_{yz}\right) \cdot \hat{z}_{Jo} = 0$$

The characteristic equation is a polynomial of the fourth degree:

$$a^2\left(\frac{\lambda}{\omega}\right)^4 + a^2 \cdot A_3\left(\frac{\lambda}{\omega}\right)^3 + (a \cdot A_4 + A_2) \cdot \left(\frac{\lambda}{\omega}\right)^2 + \quad (37)$$
$$+ A_1\left(\frac{\lambda}{\omega}\right) + A_0 = 0$$

The dimensionless parameters $A_i$, $i = 0.4$ are the influence factors and they have the following form:

$$A_0 = \gamma_{zz} \cdot \gamma_{yy} - \gamma_{yz} \cdot \gamma_{zy} \quad (38)$$
$$A_1 = \beta_{zz} \cdot \gamma_{yy} + \beta_{yy} \cdot \gamma_{zz} - (\beta_{zy} \cdot \gamma_{yz} + \beta_{yz} \cdot \gamma_{zy})$$
$$A_2 = \beta_{zz} \cdot \beta_{yy} - \beta_{yz} \cdot \beta_{zy}$$
$$A_3 = \beta_{zz} + \beta_{yy}$$
$$A_4 = \gamma_{zz} + \gamma_{yy}$$

The parameter $a$ is $a = \frac{S_O \cdot C}{g} \cdot \omega^2$. The stability condition for Equation (37) is:

$$a^2 \cdot A_1^2 - A_1(a \cdot A_4 + A_2) \cdot a \cdot A_3 + a^2 \cdot A_3^2 \cdot A_0 \le 0 \quad (39)$$

We obtain the limit stability if we put the parameter into Equation (37), modify it, and put this equal to zero:

$$\left(\frac{S_O \cdot C}{g} \cdot \omega^2\right)^2 \cdot A_1^2 - A_1\left[\left(\frac{S_O \cdot C}{g} \cdot \omega^2\right) \cdot A_4 + A_2\right] \cdot \quad (40)$$
$$\cdot \left(\frac{S_O \cdot C}{g} \cdot \omega^2\right) \cdot A_3 + \left(\frac{S_O \cdot C}{g} \cdot \omega^2\right)^2 \cdot A_3^2 \cdot A_0 = 0$$

and finally we get the limit angular velocity of the shaft:

$$\omega_L = \sqrt{\frac{g}{S_O \cdot C} \cdot \frac{A_1 \cdot A_2 \cdot A_3}{A_1^2 - A_1 \cdot A_3 \cdot A_4 + A_0 \cdot A_3^2}} \quad (41)$$

## Results and discussion

We chose the Runge-Kutta numerical method to solve differential Equations (32, 33). For each biolubricant we made simulations with temperature 40 – 100 °C. Physical and mechanical properties of used biolubricants for simulating temperatures were defined by values of their Sommerfeld numbers. As we can see from Table 4 and 5, the values of stiffness and damping for Sommerfeld numbers 1.253 and 1.3229 at temperature 40 °C are similar to the values of corresponding dimensionless parameters in Table 6 and 7. Properties of both oils at this temperature are practically comparable. In this regard, we mention the trajectory of the shaft motion only in Figure 2. Differences in stiffness and damping are obvious in case the temperature of the oil was 100 °C and values of Sommerfeld numbers were correspondent to this temperature. The viscosity of the oil changes with rising temperature. The consequence of this is the change of stiffness and damping and the change of behaviour of the shaft in the bearing. The trajectories of the bearing are depicted in Figure 3 and 4. When simulating the revolutions $n = 90 \cdot \frac{\pi}{\omega}$, we can see that the trajectory of the shaft is stabilising as shown in Figure 5. For both higher values of Sommerfeld numbers, the trajectories are nearly identical. For comparison, we present the state that will happen if we use the Ocvirk solution when we put $\gamma_{yy} = \gamma_{zz} = 0$ and $\beta_{yz} = \beta_{zy} = 0$. Here can be seen a chaotic motion of the shaft at higher values of Sommerfeld numbers. Properties of both examined biolubricants have almost the same influence on the stability of the shaft motion in the bearing. Stiffness and damping properties of both oils are comparable.

**Table 8** Maximum and minimum values of shaft centre displacement

| Displacement in mm (1) | Sommerfeld number (2) | | | | |
|---|---|---|---|---|---|
| | 1,253 | 7,0273 | 1,3229 | 7,526 | 7,526 $\left(n = 90\frac{\pi}{\omega}\right)$ |
| $y_{Jmax}$ | $2.674 \cdot 10^{-3}$ | $2.2 \cdot 10^{-3}$ | $2.432 \cdot 10^{-3}$ | $2.22 \cdot 10^{-3}$ | $2.432 \cdot 10^{-3}$ |
| $y_{Jmin}$ | 0.014 | $-2.395 \cdot 10^{-3}$ | 0.012 | $-2.395 \cdot 10^{-3}$ | $-2.419 \cdot 10^{-3}$ |
| $z_{Jmax}$ | 0.014 | 0.012 | 0.012 | 0.012 | 0.012 |
| $z_{Jmin}$ | -0.014 | -0.012 | -0.012 | -0.012 | -0.012 |

**Tabuľka 8** Maximálne a minimálne hodnoty trajektórie stredu hriadeľa
(1) premiestnenie, (2) sommerfeldovo číslo

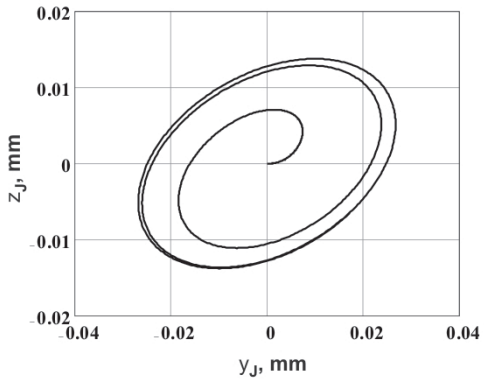


**Figure 2** Trajectories of the shaft centre at $S_0$ = 1.253
**Obrázok 2** Trajektórie stredu hriadeľa pri $S_0$ = 1,253

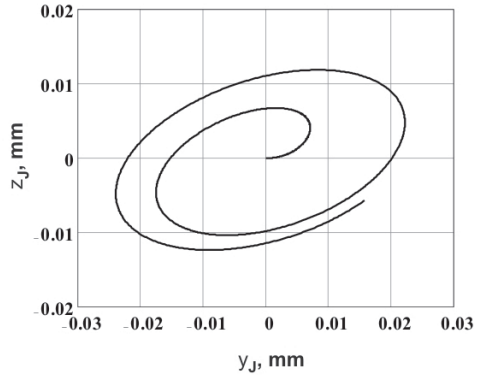


**Figure 3** Trajectories of the shaft centre at $S_0$ = 7.0273
**Obrázok 3** Trajektórie stredu hriadeľa pri $S_0$ = 7,0273

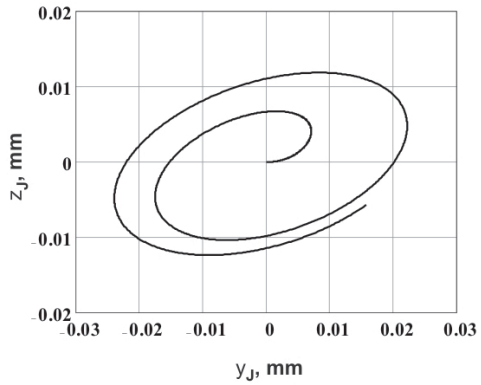


**Figure 4** Trajectories of the shaft centre at $S_0$ = 7.526
**Obrázok 4** Trajektórie stredu hriadeľa pri $S_0$ = 7,526

If we apply the Ocvirk solution for an infinitely short shaft, we obtain chaotic trajectories of the shaft centre which leads to the creation of frequency ranges, which would activate the resonance of the joint and it would cause its damage. The continuances are depicted in Figure 6 and 7.

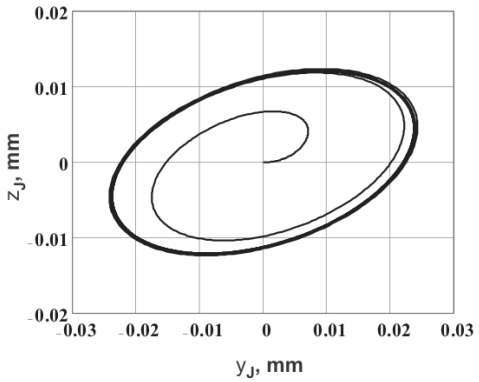


**Figure 5** Trajectories of the shaft centre at $S_0$ = 7.526 and $n = 90\frac{\pi}{\omega}$
**Obrázok 5** Trajektórie stredu hriadeľa pri $S_0$ = 7,526 and $n = 90\frac{\pi}{\omega}$

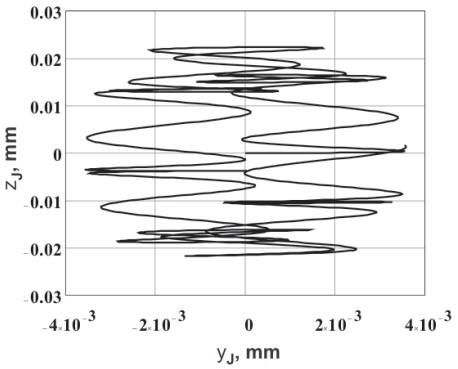


**Figure 6** Trajectories of the shaft centre at $S_0$ = 7.0273
**Obrázok 6** Trajektórie stredu hriadeľa pri $S_0$ = 7,0273

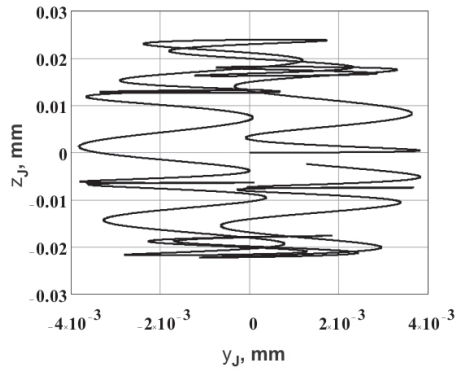


**Figure 7** Trajectories of the shaft centre at $S_0$ = 7.526
**Obrázok 7** Trajektórie stredu hriadeľa pri $S_0$ = 7,526

## Conclusion

We realized the simulation of the sliding couple where the parameter of sliding elements was evaluated according to valid methodologies. The sliding couple was lubricated with biolubricants, where the influence of properties of lubricants and of the sliding couple was defined by the Sommerfeld number. Then, we entered the formed dynamic equations with

dimensionless parameters describing the properties of lubricated sliding couple at the temperature of 40 °C and 100 °C. Following the performed simulations, we came to conclusions that the direct stiffness elements, $k_{yy}$ and $k_{zz}$, become negligible in comparison with the cross-coupled stiffness elements, $k_{yz}$ and $k_{zy}$, the direct damping elements, $c_{yy}$ and $c_{zz}$, incline to a non-zero limit, whereas the cross-coupled damping elements, $c_{yz}$ and $c_{zy}$, tend to zero. A shaft bearing must have a radial restoring force so that it has a finite stability threshold. If the shaft is operating at zero eccentricity, or if it is not allowed for the fluid film to cavitate, then the principal stiffness element vanishes, the shaft is inherently unstable, and the system will exhibit a half frequency whirl. It is known that the major sources of instability are the cross-coupled stiffness elements $k_{yz}$ and $k_{zy}$. The cross-coupled element $k_{zy}$ must be negative in order to generate instability. The largest degree of instability occurs when $k_{yz} = -k_{zy}$. The system stability rapidly improves in case $k_{yz}$ becomes negative. The greatest values of the deviation were observed in the direction with respect to $y$ axes. The motion oriented to $z$ axes was relatively consolidated. The introduced methodology is suitable for assessment of the influence of biolubricants on the stability of the shaft motion in the bearing.

## Súhrn

Zaoberali sme sa matematickou analýzou klznej dvojice, ktorá je mazaná rôznymi typmi biomazív a simuláciou stability pohybu hriadeľa v kluznom ložisku. Stabilitu otáčajúceho sa hriadeľa sme popísali systémom diferenciálnych rovníc a riešili numericky. Pre zjednodušenie matematického popisu sme použili Sommerfeldove číslo, ktorým sme definovali fyzikálne vlastnosti každého použitého biomaziva. Na stanovenie Sommerfeldovho čísla sme použili technické parametre olejov MOL Traktol NH Ultra, MOL Farm UTTO Synt. Zaťažovací cyklus v simulácii bol stanovený v rozsahu 200 – 1 000 N. Materiál hriadeľa bola kalená a popustená oceľ 12 050. Použité klzné ložisko bolo B30/38x30 STN 02 3496. Pre každý typ biomaziva a rotujúceho hriadeľa sme vypočítali trajektóriu pohybu a stanovili podmienky stability. Simulácie sa uskutočnili pri teplote 40 – 100 °C. Vlastnosti oboch skúmaných biomazív majú takmer rovnaký vplyv na stabilitu pohybu hriadeľa v ložisku. Tuhostné a tlmiace vlastnosti oboch olejov sú porovnateľné.

**Kľúčové slová:** matematické modelovanie, klzné ložisko, biomazivá

## References

FIALA, J. – SVOBODA, P. – ŠŤASTNÝ, K. 1989. Strojnické tabulky 3. Praha : SNTL. 704 s. ISBN 80-03-00151-X.

GENTA, G. 2005. Dynamics of Rotating Systems. New York : Springer Science + Business Media Inc. 660 p. ISBN 0-387-20936-0.

GASCH,R. – PFÜTZNER, H. 1975. Rotordynamik – Eine Einführung. Berlin/Heideberg : Springer Verlag. 188 p. ISBN 978-0387070469.

GOMEZ-MANCILLA, J. – NOSOV, V. – SILVA – NAVARRO, G. 2005. Rotor – Bearing System Stability Performance Comparing Hybrid versus Conventional Bearings. In: International Journal of Rotating Machinery, 2005, no. 1, p. 16 – 22. ISSN 1023-621X.

KADNÁR, M. – RUSNÁK, J. – KUČERA, M. 2007. Analýza kritických frekvencií pri skúškach na skúšobnom stroji Tribotestor. In: Acta technologica agriculturae, roč. 10, 2007, č. 3 – 4, s. 66 – 69. ISSN 1335-2555.

MALVANO, R. – VATTA, F. – VIGLIANI, A. 1999. Lubricated Plane Slider Bearing : Analytic and Numerical Approach. In: Meccanica, vol. 34, 1999, no. 4, p. 237 – 250. ISSN 1572-9648.

NATARAJ, C. – HARSHA, S. P. 2008. The effect of bearing cage run-out on the nonlinear dynamics of a rotating shaft. In.: Communications in Nonlinear Science and Numerical Simulation, vol. 13, 2008, no. 4, p. 822 – 838.

VOZÁROVÁ, V. 2009. Methods of the thermal stability investigation of biological materials. In: BioPhys Spring 2009 : abstracts, 8th International workshop for young scientists, May 21 – 22, 2009, Lublin : Institute of Agrophysics, 2010. ISBN 978-83-89969-41-5.

VOZÁROVÁ, V. – BOJDA, J. 2008. Fyzikálne vlastnosti biopalív z hľadiska posudzovania ich kvality. In Technika v technológiách agrosektora 2008 : zborník vedeckých prác z medzinárodnej vedeckej konferencie poriadanej pod záštitou ministra hospodárstva vlády SR Ľubomíra Jahnátka, Nitra, 26. november 2008. Nitra : SPU, 2008, s. 132 – 136. ISBN 978-80-552-0147-4.

WANG, J. K. – KHONSARI, M.M. 2006. A new derivation for journal bearing stiffness and damping coefficients in polar coordinates. In Journal of Sound and Vibration, vol. 290, 2006, no. 1 – 2, p. 500 – 507. ISSN 0022-460X.

ŽARNOVSKÝ, J. 1998. Technická diagnostika, výpočtová technika z pohľadu starostlivosti o poľnohospodársku techniku. In Zborník z I. medzinárodnej vedeckej konferencie mladých 1998 : Račkova Dolina – Západné Tatry 5. – 7. 10. 1998. Nitra : SPU, 1998, s. 194 – 197. ISBN 80-7137-527-6.

Contact address:
doc. Ing. Jozef Rédl, PhD., Ing. Veronika Váliková, Ing. Michal Kročko, Department of Machine Design, Faculty of Engineering, Slovak University of Agriculture in Nitra, Tr. A. Hlinku 2, 949 76 Nitra, e-mail: jozef.redl@uniag.sk, xvalikovav@is.uniag.sk, michal.krocko@uniag.sk

Acta technologica agriculturae 2
Nitra, Slovaca Universitas Agriculturae Nitriae, 2012, p. 53–56

# SETTING OF PARAMETERS OF A PLASTIC FILM PRODUCTION PROCESS
# STANOVENIE PARAMETROV VÝROBNÉHO PROCESU PLASTICKEJ FÓLIE

Maroš KORENKO, Róbert DRLIČKA, Tomáš KUČERKA

Slovak University of Agriculture in Nitra, Slovak Republic

BoPET film industry development is influenced by similar forces as other industries, i.e. competition particularly from Chinese and Indian manufacturers. Cooperation is one of the strategies leading to success. This paper deals with production line setting for one of the leaders in BoPET film production in its cooperating Chinese company. It describes the film production process, production line and its elements, assembling and run-in, together with production parameter setting. Process parameters are observed and measured on-line, but the quality assessment is based on results of film tests according to an applicable standard for tests.

**Keywords**: optimisation, quality, process, production line, BoPET film

Every day in our life we use products provided/packed in various covers/packaging. Demands on the film type and quality are determined particularly by its purpose and use in practice, in case of foods, technical use, automotive industry, etc. There are many different production lines for this field on the market. An accomplishment of high operational reliability criteria of the line is determined by its design and manufacturing. The process of assembling of the whole production line is very important together with start-up and run-in. At these stages, all needed attributes have to be observed to achieve customers' and production line requirements from the beginning to fulfil the highest quality parameters. The line produces a wide range of BoPET films. Optimisation achieved great importance in last decades. Recently, quality management has become a strategic issue in the top management of all customer-oriented organizations. Removing non-conformities after the production process is inefficient and financially much more expensive than prevention in the form of a quality management system. Therefore, it is important to analyse internal processes that leads to the disclosure of defects and hidden reserves for improving the functioning of the entire organization (Savov and Džupina, 2007).

## Material and methods

### BoPET characteristics

Polyester belongs to a wide group of organic high-molecular polymers. Contemporary, films of polyethylene terephtalate and aromatic polyester dominate the area of industrial polyester films. Polyethylene terephtalate films are strong, tight and flexible/elastic, with a low absorption rate, low gas leakiness and good resistance to chemical materials. Industry applications benefit from excellent dielectric characteristics.

In present time, polyethylene terephtalate is made mostly from pure terephtalate acid (PTA) and monoethylene glycol (MEG) using polycondensation.

The abbreviation BoPET means biaxially oriented polyethylene terephtalate. The range of industry applications covers the thicknesses from less than 1 μm up to 350 μm. The most common thicknesses are shown in Table 1.

**Table 1** Thickness of BoPET and relevant application

| Thickness in μm (1) | Application (2) |
|---|---|
| 1 / 2 / 2.5 / 5 | capacitors |
| 5.8 / 6 / 7.5 / 9 | audio-video products, technical use |
| 8/10 / 11.5 / 12 / 15 | packaging, metallizing, use in electrical engineering industry |
| 18 / 20 / 23 / 25 | versatile application, packaging, etc. |
| 36 / 40 / 50 / 75 | graphics, diskettes, etc. |
| 100 / 125 / 175 / 190 | graphic cards, micro films, LCDs |
| 200 / 259 / 350 | electric insulations, reinforcements |

**Tabuľka 1** Použitie BoPET fólie podľa jej hrúbky
(1) hrúbka v μm, (2) použitie

### BoPET film processing

The production line is designed for biaxially oriented film production in a two-stage process. Biaxially oriented means the film is stretched in two main directions, oriented in a 90° angle. Two-stage stretching means the film is manufactured in two stages, in a longitudinal direction (MD) in the first stage and transversal direction (TD) in the second stage.

### Manufacturing process

The base stock is polypropylene granulate poured to preheated extruders, screwed mills. Extruders press the granulate to a semi-liquid transparent melt form. This melting is pushed to an extruding nozzle using a gear pump. The base element of the nozzle is an aperture. The aperture size is controlled in the whole length using an electric heating of elements. These elements change the length according to own temperature and directly influence the aperture width.

After extruding through the nozzle, the melting proceeds with a temperature of approximately 250 °C to a cooling cylinder with a temperature of approximately 80 °C. The melting leaves the cylinder area in the form of film reaching the width of several millimetres and enters the section of longitudinal orientation (MDO). This section is composed of a large-scale cylinder system with cylinder speeding-up causing longitudinal film stretch. This is the first stage of orientation in the longitudinal direction. This section is

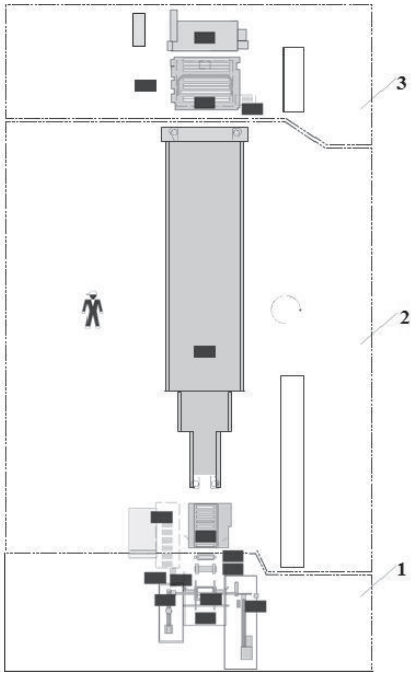


**Figure 1** Layout of the BoPET line components
1 – raw material and cast film, 2 – stretching, 3 – finishing and winding

**Obrázok 1** Schéma prvkov linky pre BoPET
1 – vstupná surovina a východisková fólia, 2 – predlžovanie, 3 – dokončovanie a navíjanie

composed of three zones. In the first zone, the film in heated by tempered cylinders; in the middle zone, the film is stretched up; and in the third zone, it is cooled again. These processes, the rate and speed of cooling influence significantly the resultant film quality. Orientation in the transversal direction comes up then in the device of a length of approximately 50 m (TDO).

The orientation chain is the central element, clamping the film wĕmith many flaps on the margins and stretching it to wideness. The film temperature has to be appropriate for forming (from 160 °C to 190 °C), but it must not cause sticking on flaps. The film width at the beginning is 1 m; at the end, it is stretched to a width from 5 m up to 10 m thanks to the chain at velocity 550 m/min. The highest attention is paid to film stretching uniformity, dependent not only on the stretching process but also mixture consistence quality. The film then runs into the warming and cooling cylinders section where the film parameters are stabilised. A winder unit is the last section. Rolls with a loaded film ('jumbo rolls') are then moved to cutter machines. These rolls are cut to shorter rolls according to customers' demands.

The main process units:

- charging of granulates,
- extrusion unit and die,
- cast film unit,
- thickness gauge,
- MDO machine direction orienter,
- TDO transverse direction orienter,
- pull roll unit,
- winder unit.

The composition of the BoPET production line components assembled to sections is shown in Figure 1.

## Customers' requirements

The basis for BoPET film assessment on the roller lies in qualitative parameters. The values and testing conditions are shown in the following Tables.

**Table 2** Guaranteed output for 8.7 m of the BoPET film net width

| Thickness in μm (1) | Speed (approximately) in $m.min^{-1}$ (2) | Nominal net output in $kg.h^{-1}$ (3) |
|---|---|---|
| 8 | 320 | 1,864 |
| 10 | 350 | 2,550 |
| 12 | 410 | 3,583 |
| 15 | 339 | 3,600 |
| 20 | 254 | 3,700 |
| 30 | 169 | 3,700 |
| 36 | 141 | 3,700 |
| 50 | 100 | 3,700 |
| 75 | 68 | 3,700 |

**Tabuľka 2** Garantovaný výstup pre BoPET fóliu s čistou šírkou 8,7 m
(1) hrúbka in μm, (2) rýchlosť (približná) v $m.min^{-1}$, (3) nominálny čistý výstup

**Table 3** General characteristics

| Category (1) | Guaranteed characteristics (2) | | | | Unit (3) |
|---|---|---|---|---|---|
| Nominal thickness | 12 – 15 | 16 – 36 | 37 – 50 | 51 – 75 | μm |
| Thickness tolerance | | | | | |
| Online measurement (TCE) | ± 2.5 | ± 2.5 | ± 2.5 | ± 2.5 | % |
| Error in average layer thickness | +1.5 | +1.5 | +1.5 | +1.5 | % |
| Tensile strength – MD<br>– TD | 220<br>230 | 220<br>220 | 200<br>200 | 180<br>180 | MPa<br>MPa |
| Strain at fracture MD | 100 – 140 | 150 | 160 | 180 | % |
| Young's modulus – MD<br>– TD | 4,000<br>4,200 | 4,000<br>4,200 | 3,800<br>4,000 | 3,800<br>4,000 | MPa<br>MPa |
| Maximum thermal shrinkage – MD<br>– TD | 2.0<br>0.5 | 2.0<br>0.5 | 2.0<br>0.5 | 2.0<br>0.5 | % |
| Maximum friction coefficient | 0.55 | 0.55 | 0.5 | 0.5 | – |
| Maximum clarity | 2.0 | 2.0 | 2.0 | 2.5 | – |
| Minimum glare | 110 | 110 | 110 | 110 | – |

**Tabuľka 3** Všeobecné charakteristiky
(1) kategória, (2) garantované charakteristiky, (3) jednotka

During installation of the BoPET production line, we have gathered necessary data for objective achievement – process parameter optimisation. After a successful putting of the technological line into operation, film samples from jumbo rolls are sampled in size A4. Results are recorded in operation using an operational software, but laboratory tests are performed as well. Qualified staff conducts the tests in internal conditions of the manufacturing organization. The samples taken from roll No 12 were chosen as an example and tested in the directions MD and TD for tensile strength assessment using a device Zwick Roell at testing speed 100 mm.min$^{-1}$.

## Results and discussion

After a successful setup of the production line for the BoPET film, the start-up stage was launched. The Tables below prove the fulfilment of customers' requirements and warranty criteria.

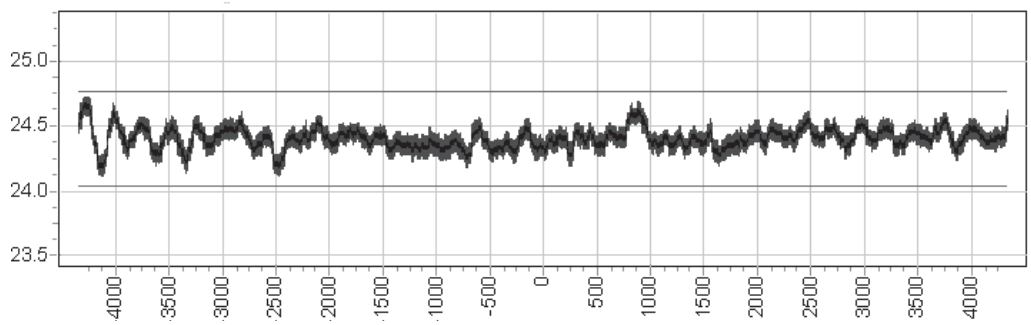


| Thickness minimum (1) | Average thickness (2) | Thickness maximum (3) | 2-Sigma in μm | 2-Sigma in % |
|---|---|---|---|---|
| 24.19 | 24.40 | 24.66 | 0.144 | 0.589 |

**Figure 2** Actual profile
**Obrázok 2** Skutočný profil
(1) minimálna hrúbka, (2) priemerná hrúbka, (3) maximálna hrúbka

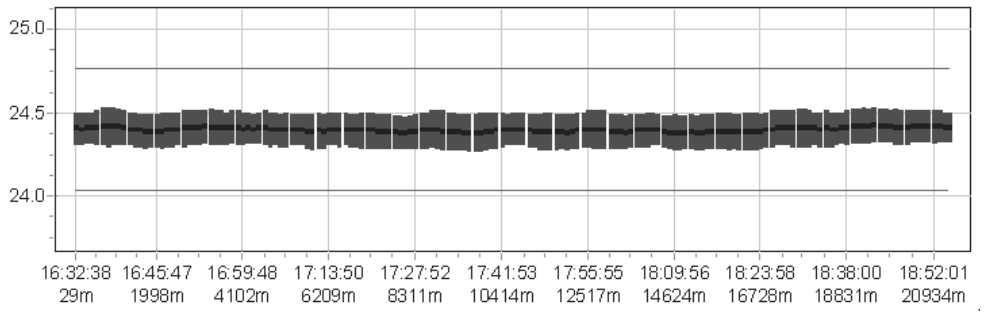


| Thickness minimum (1) | Average thickness (2) | Thickness maximum (3) | 2-Sigma in μm | 2-Sigma in % |
|---|---|---|---|---|
| 24.38 | 24.40 | 24.43 | 0.02 | 0.09 |

**Figure 3** Actual trend
**Obrázok 3** Skutočný vývoj
(1) minimálna hrúbka, (2) priemerná hrúbka, (3) maximálna hrúbka

**Table 4** Characteristics report for film thickness 25 μm

| Measurement Record (1) | | | | | | | |
|---|---|---|---|---|---|---|---|
| Roll ID | 0A1109291632 | Product | 25 mic | | Diameter | 1,059.4 | mm |
| Roll name | NA | Composition | NA | | Weight | 6,277 | kg |
| Production | P0A1109290701 | Quality | | | Density | 95.5 | % |
| Status | good roll | | | | Net output | 2,670 | kg.h$^{-1}$ |
| Start | 29/09/2011 16:32 | Actual thickness | 24.4 | μm | No of scans | 163 | |
| Finish | 29/09/2011 18:55 | Set thickness | 24.4 | μm | Speed | 150 | m.min$^{-1}$ |
| Project | PEF | Length | 21,299 | m | 2-Sigma TD | 0.144 | μm |
| Operation | start-up | Width | 8,700 | mm | 2-Sigma MD | | % |

**Tabuľka 4** Záznam vlastností fólie hrúbky 25 μm
(1) záznam merania

**Table 5** Characteristics report for film thickness 12 μm

| Measurement Record (1) | | | | | | | |
|---|---|---|---|---|---|---|---|
| Roll ID | 0A1110050045 | Product | 12 mic | | Diameter | 1,130.2 | mm |
| Roll name | NA | Composition | NA | | Weight | 7,183 | kg |
| Production | P0A1110041453 | Quality | | | Density | 89.1 | % |
| Status | good roll | | | | Net output | 2,206 | $kg.h^{-1}$ |
| Start | 05/10/2011 00:45 | Actual thickness | 12.19 | μm | Nr. of scans | 224 | |
| Finish | 05/10/2011 04:02 | Set thickness | 12.10 | μm | Speed | 248 | $m.min^{-1}$ |
| Project | PEF | Length | 48,697 | m | 2-Sigma TD | 0.052 | μm |
| Operation | start-up step 2 | Width | 8,700 | mm | 2-Sigma MD | 0.209 | % |

**Tabuľka 5** Záznam vlastností fólie hrúbky 12 μm
(1) záznam merania

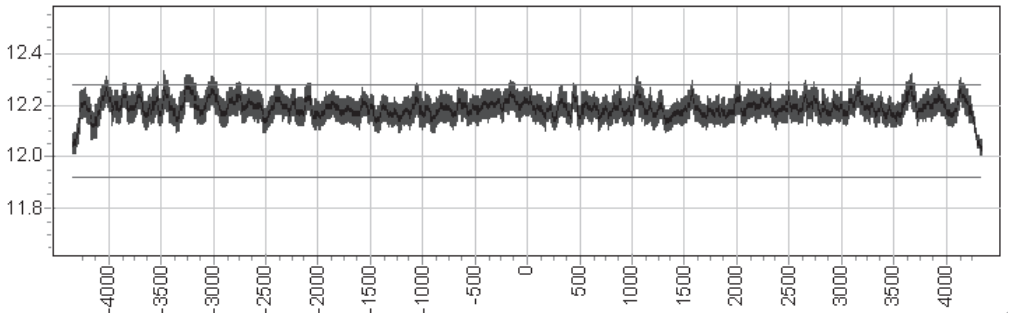


| Thickness minimum (1) | Average thickness (2) | Thickness maximum (3) | 2-Sigma in μm | 2-Sigma in % |
|---|---|---|---|---|
| 12.09 | 12.19 | 12.27 | 0.052 | 0.43 |

**Figure 4** Actual profile
**Obrázok 4** Skutočný profil
(1) minimálna hrúbka, (2) priemerná hrúbka, (3) maximálna hrúbka

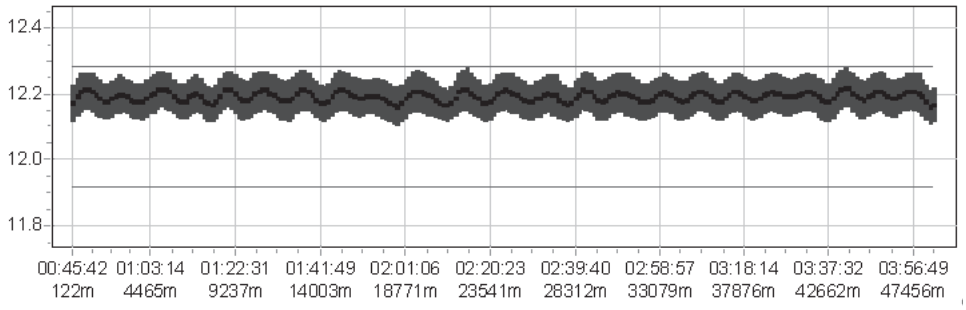


| Thickness minimum (1) | Average thickness (2) | Thickness maximum (3) | 2-Sigma in μm | 2-Sigma in % |
|---|---|---|---|---|
| 12.16 | 12.19 | 12.22 | 0.03 | 0.21 |

**Figure 5** Actual trend
**Obrázok 5** Skutočný vývoj
(1) minimálna hrúbka, (2) priemerná hrúbka, (3) maximálna hrúbka

Required characteristics and film properties steadiness has been achieved by optimisation. After successful run-in, the velocity was increased to 250 $m.min^{-1}$, and a higher speed brought a thickness fall to 12 μm. The guaranteed values obtained in the process are shown in the following Tables and Figures.

### Laboratory tests in the MD and TD direction

Tests are performed according to the specification of the international standard DIN 50014 23/50-2. The air temperature is 23 ± 2 °C and humidity 50 ± 6 %. Samples were taken from roll No 12, made at production speed 150 $m.min^{-1}$ and thickness 25 μm. Tests were performed with five samples in the MD and TD directions for tensile strength determination, using the device Zwick Roell and testing speed 100 $m.min^{-1}$. The test results in the MD and TD direction are shown in Figures 5 and 6, respectively.

### Conclusions

The table of guaranteed film characteristics provides the range of parameters defining the quality level designated A. It is very important the thickness values respond to the nominal film